High-temperature magnetization reversal in the inertial regime

I. Makhfudz,[1,2] Y. Hajati,[3] and E. Olive[1]
[1]*GREMAN, UMR 7347, Université de Tours-CNRS, INSA Centre Val de Loire, Parc de Grandmont, 37200 Tours, France*
[2]*IM2NP, UMR CNRS 7334, Aix-Marseille Université, 13013 Marseille, France*
[3]*Department of Physics, Faculty of Science, Shahid Chamran University of Ahvaz, 6135743135 Ahvaz, Iran*

(Received 3 May 2022; revised 29 September 2022; accepted 6 October 2022; published 17 October 2022)

Motivated by the remarkable experimental observation of all-optical femtosecond-scale magnetization reversal at relatively high temperatures, a stochastic inertial Landau-Lifshitz-Gilbert-Bloch (iLLGB) equation is written to describe nonequilibrium magnetization dynamics in ferromagnets at elevated temperatures and at short enough timescales that an inertial effect manifests. The effect of thermal agitations is described by a Fokker-Planck equation derived from the iLLGB equation including the longitudinal relaxation effect, which is solved with perturbation theory valid at elevated temperatures. Considering a uniaxially symmetric ferromagnet with uniaxial anisotropy, a thermal diffusion-driven exponential mode and alternating field-driven nutation mode of stable magnetization reversal are identified. Our theory proposes a magnetization reversal mechanism based entirely on transfer of angular momentum to the local magnetization, but which takes into account thermal fluctuations and inertial effect at the same time. The theory explains several key observations in all-optical magnetization reversal experiments; the absence of the need for a static field, the subpicosecond switching timescale, the relative roles of thermal and field effects, and the relevance of circularly polarized light. Our results have direct implications for magnetic recording devices operating close to room temperatures and in the ultrafast regime.

DOI: 10.1103/PhysRevB.106.134415

I. INTRODUCTION

Understanding magnetization dynamics in the ultrafast regime and at elevated temperatures is a key challenge in realizing high-speed magnetic devices operating at ambient temperature. Magnetization dynamics in ferromagnets has so far been studied using the Landau-Lifshitz-Gilbert equation assuming that the magnetization magnitude is constant, valid at low enough temperatures (relative to Curie temperature T_C) [1,2]. An improvement of this approach takes into account the longitudinal mode corresponding to the change in the magnitude of the magnetization using Landau-Lifshitz-Bloch equation that is valid even at high temperatures, below and above the T_C of ferromagnets [3–5]. Building on the free-energy description of ferromagnets [6], the effect of thermal fluctuations and longitudinal relaxation were then studied [7], highlighting the general importance of fluctuations in magnetic phase transitions [8]. All these studies assume that magnetization dynamics is slow enough.

Remarkable development in recent decades has demonstrated theoretically [9,10] and experimentally [11] the existence of magnetic inertial effect in the magnetization dynamics in ferromagnets at short timescales. Its effect is analyzed using the so-called inertial Landau-Lifshitz-Gilbert equation and shown to give rise to a type of collective mode called nutation for a single spin [9,12,13] and nutation wave for lattice of spins [14,15]. The formalism has been extended to include the thermal fluctuations effect [16]. From a practical perspective, inertial magnetization dynamics has been suggested to be applied to magnetic switching technique [17]. However, all these studies still assume fixed magnitude of magnetization that underlies the employed inertial Landau-Lifshitz-Gilbert equation. A Landau-Lifshitz-Bloch type of description exists, but does not address the inertial regime [18,19].

From an experimental point of view, the study of ultrafast magnetization dynamics has become an active research area of its own, especially since the experimental observation of a femtosecond timescale demagnetization process [20,21]. Further experimental progress following after that produced important observations that call for theoretical description beyond Landau-Lifshitz-Gilbert theory. One example is the relative importance of the role of temperature and applied field in driving the dynamics [22–24]. Furthermore, remarkable recent experimental developments show that magnetization reversal can be realized *at zero static field* using a nonthermal all-optical method [25,26] which nevertheless operates at relatively high temperatures (that is, not close to $T = 0$ K), as opposed to thermal-assisted laser-induced heating magnetization reversal [23] or demagnetization processes [20]. This advance has unfolded while the microscopic mechanism responsible for the ultrafast magnetism phenomena has come under intense scrutiny [22,27], which can in fact be all-optical [28,29], even though more complicated scenarios exist [30–33], while the all-optical mechanism has again been demonstrated by more recent studies [34].

In this paper, we develop an inertial Landau-Lifshitz-Gilbert-Bloch (iLLGB) equation to study magnetization dynamics in the inertial regime at elevated temperatures not far from T_C, taking into account longitudinal relaxation and

thermal fluctuations. While strong thermal fluctuations at elevated temperatures are expected to destroy any stable magnetization reversal mechanism, the present paper shows that this restriction does not apply to inertial magnetization dynamics; an intriguing type of switching mode originating from the inertial effect with a subpicosecond timescale that survives thermal agitations is unraveled, requiring only an ac field of high-enough frequency and amplitude for its manifestation. Our theory also provides a natural explanation for some of the key observations of all-optical magnetic switching experiments.

This paper starts with an equation of motion proposed to be appropriate for describing magnetization dynamics in high temperatures below Curie temperature and in the ultrafast regime where inertial effect manifests in Sec. II. The corresponding Fokker-Planck equation describing stochastic dynamics out of equilibrium in ultrafast regime is derived from the equation of motion in Sec. III. The magnetic potential governing the energetics of the magnetization dynamics and the corresponding modes of magnetization reversal are given in Sec. IV. The solutions of the Fokker-Planck equation in the steady-state and nonsteady state subject to constant magnetic potential are given in Sec. V while the solution for the actual magnetic potential is given in Sec. VI. The speeds of two principal modes of magnetization reversal are given in Sec. VII. The paper ends with Discussion and Conclusions.

II. THE INERTIAL LANDAU-LIFSHITZ-GILBERT-BLOCH EQUATION

The dynamics of magnetization in ferromagnets at elevated temperatures and in the inertial regime is supposed to be described by an inertial Landau-Lifshitz-Gilbert-Bloch (iLLGB) equation which can be written as

$$\dot{\mathbf{m}} = \gamma_0(\mathbf{m}\times(\mathbf{H}_{\rm eff}+\mathbf{h}(t))) + \frac{\gamma_0\alpha_\parallel}{m^2}(\mathbf{m}\cdot(\mathbf{H}_{\rm eff}+\mathbf{h}(t)))\mathbf{m} - \frac{\alpha_\perp}{m^2}[\mathbf{m}\times\dot{\mathbf{m}}+\tau\mathbf{m}\times\mathbf{m}], \quad (1)$$

where γ_0 is the gyromagnetic constant, $\mathbf{m}$ is the magnetization vector with temperature-dependent magnitude normalized to its zero temperature (saturation) value $\mathbf{m}=\mathbf{M}/M_s$, where $M_s=|\mathbf{M}(T=0)|$ and is also time dependent, appropriate to describe magnetization dynamics near Curie temperature [35], $\dot{\mathbf{m}}=\partial\mathbf{m}/\partial t$, $\mathbf{m}=\partial^2\mathbf{m}/\partial t^2$, $\mathbf{H}_{\rm eff}=-\partial V[\mathbf{m}]/\partial\mathbf{m}$, where $V[\mathbf{m}]$ is a magnetic potential energy to be defined in Sec. IV, and $\mathbf{h}(t)$ the stochastic field used to describe thermal fluctuations (agitations) satisfying a purely random field's white-noise properties [36],

$$\langle h_i(t)\rangle = 0,\ \langle h_i(t)h_j(t+\tau)\rangle = \mu\delta_{ij}\delta(\tau), \quad (2)$$

while $\alpha_\parallel(\alpha_\perp)$ are the effective damping coefficients along (perpendicular to) the direction of $\mathbf{m}$, both of which are temperature dependent [7,37], τ is a timescale that separates the inertial $t\ll\tau$ and noninertial (slow, adiabatic) $t\gg\tau$ regimes in timescale while $\mu=2\alpha_\perp k_BT/(\gamma_0 vM_s)$ is the white noise constant. The first term on the right-hand side of Eq. (1) (proportional to γ_0) represents the gyroscopic torque due to the effective magnetic field, the second one (proportional to $\alpha_\parallel$) is the Bloch term representing longitudinal relaxation necessary to describe magnetization dynamics at elevated temperatures, while the last two terms (proportional to $\alpha_\perp$) represent, respectively, the Gilbert damping and inertial effects. Notably, the second term in Eq. (1) (proportional to $\alpha_\parallel$) generates a torque along the direction of $\mathbf{m}$; applying an effective field $\mathbf{H}_{\rm eff}$ antiparallel to $\mathbf{m}$ tends to reverse the $\mathbf{m}$. This effect is absent in Landau-Lifshitz-Gilbert theory.

In the present paper, we will derive Fokker-Planck equation using the heuristic approach of Brown [36], shown by later studies to be justified under appropriate conditions and gives a unique Fokker-Planck equation for stochastic Landau-Lifshitz-Gilbert theory [18,19]. In our paper, a unique Fokker-Planck equation corresponding to continuity equation (conservation of Brown particle current) is postulated *a priori* to emerge independent of choices of stochastic variables, which is *a posteriori* demonstrated to give Boltzmann distribution in statistical equilibrium. As we will apply an alternating magnetic field that drives the system out of equilibrium, fluctuation-dissipation theorem is not imposed.

Working in a spherical coordinate to be concrete, we can write $\mathbf{m}=m_r(\sin\theta\cos\phi,\sin\theta\sin\phi,\cos\theta)$, with $m_r=|\mathbf{m}|$, where $\mathbf{m}$ in general form has been defined earlier following Eq. (1). Adopting the physical picture put forward in the elegant theory of Brown [36], the tip of the $\mathbf{m}$ vector is treated as an effective (magnetic) charge. Since in our theory the magnitude of the $\mathbf{M}$ vector is not fixed, that is, the m_r may depend on time (in addition to temperature), the charge density is defined as density per unit volume which we will denote with ρ, resulting in current density when moving with velocity $\mathbf{v}$ given by $\mathbf{J}=\rho\mathbf{v}$ where $\mathbf{v}=\partial\mathbf{m}/\partial t=\partial\mathbf{M}/\partial t/M_s$, when thermal fluctuations (agitations) are neglected. Thermal agitations are then included by adding a term of the form $-k'\nabla\rho$ into the magnetic current density, giving a total current density of the Brown particle,

$$\mathbf{J}=\rho\frac{\partial\mathbf{m}}{\partial t}-k'\nabla\rho, \quad (3)$$

where the second term on the right-hand side reflects the stochastic effect of thermal fluctuations. Within Brown's original framework [36],

$$k'\simeq\frac{k_BT}{v}\frac{\alpha_\perp\gamma_0}{M_s}, \quad (4)$$

where k_B is Boltzmann constant, v the volume of the magnetic single domain, and the approximate equality assumes $\alpha_\perp^2\ll 1$. In this paper, we will take v to be the volume of the unit cell of the crystal lattice of the (elemental) ferromagnets to be considered as examples for application of our theory, since the unit cell gives a characteristic volume for the material. Since the unit cell is the elementary volume of the material, our theory can be directly extended and applied to larger systems made up of such atomic-scale unit cells, such as magnetic nanoparticles and thin films. This assumes a certain degree of correlation between the microscopic atomic moments living in different unit cells that make up the magnetization at the macroscopic level.

III. FOKKER-PLANCK EQUATION

The first goal is to obtain a Fokker-Planck equation for the Brown particle density ρ. As established in Ref. [36], the Fokker-Planck equation eventually reduces to the continuity equation

$$\frac{\partial \rho}{\partial t} + \nabla \cdot \mathbf{J} = 0, \tag{5}$$

which thus requires the expression for the current volume density $\mathbf{J}$ in spherical coordinates. Evaluating $\mathbf{J}$ from Eq. (3) with $d\mathbf{m}/dt$ derived using Eq. (1) and spherical coordinate representation of $\mathbf{m}$, we obtain

$$\mathbf{J} \equiv (J_r, J_\theta, J_\phi) = (L_r, L_\theta, L_\phi)\rho - k'\left(\frac{\partial \rho}{\partial m_r}, \frac{\frac{\partial \rho}{\partial \theta}}{m_r}, \frac{\frac{\partial \rho}{\partial \phi}}{m_r \sin\theta}\right), \tag{6}$$

where L_r, L_θ, L_ϕ, the detailed form of which is to be derived at the end of this section, representing the drift terms, each of which is a function of m_r, θ, ϕ, t (in the most general case) dependent on $V[\mathbf{m}]$ multiplying the density function ρ while the terms multiplying k' represent the diffusion terms. The Bloch term contributes to the radial current J_r via a term proportional to the longitudinal relaxation coefficient $\alpha_\parallel$, reflecting the fact that the dynamics involves a volumetric particle number and current densities rather than a superficial particle number and current densities used in Brown's original formulation [36].

To derive the expression for the current density $\mathbf{J}$ from the iLLGB Eq. (1), we must first transform the latter into a form such that all the time derivative terms of $\mathbf{m}$ are moved to the left-hand side of the iLLGB equation. To this end, we transform the iLLGB equation using the method normally used to translate a Landau-Lifshitz-Gilbert equation back into a Landau-Lifshitz equation. There are several ways of doing so. One of them is to substitute the whole right-hand side of the iLLGB equation for $\dot{\mathbf{m}}$ into the $\dot{\mathbf{m}}$ and $\ddot{\mathbf{m}}$ terms that appear on the right-hand side of the iLLGB equation itself. This, however, would generate an infinite series of terms with increasing higher order time derivatives of $\mathbf{m}$. A more viable approach is to multiply both sides of the iLLGB equation that allows cancellation of some (though not all) time derivative terms of $\mathbf{m}$. This can be achieved by multiplying both sides of the iLLGB equation by $(1 - (\alpha_\perp/m^2)\mathbf{m}\times)$ from the left. The resulting equation becomes

$$\begin{aligned}\dot{\mathbf{m}} = {} & \frac{\gamma_0}{1+\frac{\alpha_\perp^2}{m^2}}(\mathbf{m}\times(\mathbf{H}_{\text{eff}} + \mathbf{h}(t))) \\ & + \frac{\gamma_0 \frac{\alpha_\parallel}{m^2}}{1+\frac{\alpha_\perp^2}{m^2}}(\mathbf{m}\cdot(\mathbf{H}_{\text{eff}}) + \mathbf{h}(t))\mathbf{m} \\ & - \frac{1}{1+\frac{\alpha_\perp^2}{m^2}}\frac{\alpha_\perp}{m^2}[\gamma_0 \mathbf{m}\times(\mathbf{m}\times(\mathbf{H}_{\text{eff}} + \mathbf{h}(t))) + \tau \mathbf{m}\times\mathbf{m}] \\ & + \frac{1}{1+\frac{\alpha_\perp^2}{m^2}}\frac{\alpha_\perp^2}{m^4}[(\mathbf{m}\cdot\dot{\mathbf{m}})\mathbf{m} + \tau((\mathbf{m}\cdot\ddot{\mathbf{m}})\mathbf{m} - m^2\ddot{\mathbf{m}})],\end{aligned} \tag{7}$$

which still has time derivative terms of $\mathbf{m}$ on the right-hand side of the equation. We will proceed with approximation where we take $\dot{\mathbf{m}}$ to be given by all terms on the right-hand side that contains no time derivative and use it to obtain the corresponding expression for $\ddot{\mathbf{m}}$. We will also drop the last terms [the second line of Eq. (7) above] as they are proportional to second-order power of the expected small parameter $\alpha_\perp \ll 1$. In the rest of the derivation, we will simplify $1 + \alpha_\perp^2/m^2 \simeq 1$. justified for $\alpha_\perp^2/m^2 \ll 1$.

One can define an error factor

$$\delta = \left|1 - \frac{1}{1+\frac{\alpha_\perp^2}{(m_r^{\min})^2}}\right| \tag{8}$$

as a measure of the error introduced by the above approximation $1 + \alpha_\perp^2/m^2 \simeq 1$, where $m_r^{\min}$ is the value of m_r that minimizes the magnetic potential $V[\mathbf{m}]$, to be derived in the next section. Constraining this error factor to be smaller than a threshold value (for example, $\delta \leqslant 0.1$) sets a criterion to the temperature range, field strength, and the material parameters for which our theory can be applied since $\alpha_\perp$ and $m_r^{\min}$ are dependent on those quantities, as described in the next section. When δ goes beyond the chosen threshold value of tolerance, our simplified analysis becomes less accurate. However, this can be partially mitigated by compensating for the error in the final result. The simplest way to compensate for this error (that is, lowest order correction) will be adopted; the error factor δ will eventually be used to correct the final result of the analytical derivation, especially the physical result of main interest: the magnetization reversal rate.

The Brown particle current density vector $\mathbf{J}$ in the absence of thermal fluctuations is then given by $\mathbf{J} = \rho\dot{\mathbf{m}}$, where the $\dot{\mathbf{m}}$ is equal to the right-hand side of Eq. (1) [without the stochastic field $\mathbf{h}(t)$] expressed in the spherical coordinates. We then add the contributions of thermal fluctuations (or agitations) $\mathbf{J}^{tf} = -k'\nabla\rho$ described by a diffusion term (proportional to the gradient or spatial inhomogeneity of the magnetic charge) with its components:

$$J_r^{tf} = -k'\frac{\partial \rho}{\partial m_r}, \quad J_\theta^{tf} = -\frac{k'}{m_r}\frac{\partial \rho}{\partial \theta}, \quad J_\phi^{tf} = -\frac{k'}{m_r \sin\theta}\frac{\partial \rho}{\partial \phi}. \tag{9}$$

The total current density is given by the sum of the drift and diffusive contributions. With the details of derivation given in Appendix A, the three spherical coordinate components of the current vector are given by

$$J_r = -\rho\gamma_0\alpha_\parallel\frac{\partial V}{\partial m_r} - k'\frac{\partial \rho}{\partial m_r} = L_r\rho - k'\frac{\partial \rho}{\partial m_r}, \tag{10}$$

$$\begin{aligned} J_\theta = {} & \frac{\rho\gamma_0}{\sin\theta}\left(1 + \frac{\alpha_\perp\tau\gamma_0}{m_r}\frac{\partial V}{\partial m_r}\right)\frac{\partial V}{\partial \phi} \\ & - \rho\frac{\alpha_\perp\gamma_0}{m_r}\left(1 + \tau\frac{\partial}{\partial t}\right)\frac{\partial V}{\partial \theta} - \frac{k'}{m_r}\frac{\partial \rho}{\partial \theta} \\ = {} & L_\theta\rho - \frac{k'}{m_r}\frac{\partial \rho}{\partial \theta}, \end{aligned} \tag{11}$$

$$\begin{aligned} J_\phi = {} & -\rho\gamma_0\left(1 + \frac{\alpha_\perp\tau\gamma_0}{m_r}\frac{\partial V}{\partial m_r}\right)\frac{\partial V}{\partial \theta} \\ & - \frac{\rho\alpha_\perp\gamma_0}{m_r\sin\theta}\left(1 + \tau\frac{\partial}{\partial t}\right)\frac{\partial V}{\partial \phi} - \frac{k'}{m_r\sin\theta}\frac{\partial \rho}{\partial \phi} \\ = {} & L_\phi\rho - \frac{k'}{m_r\sin\theta}\frac{\partial \rho}{\partial \phi}, \end{aligned} \tag{12}$$

where the differential operators L_r, L_θ, L_ϕ can be easily identified from each corresponding equation.

The corresponding Fokker-Planck equation is given by

$$\frac{\partial \rho}{\partial t} + \left[\frac{\frac{\partial}{\partial m_r}\left(m_r^2 J_r\right)}{m_r^2} + \frac{\frac{\partial}{\partial \theta}(\sin\theta J_\theta)}{m_r \sin\theta} + \frac{\frac{\partial J_\phi}{\partial \phi}}{m_r \sin\theta} \right] = 0 \quad (13)$$

to be solved for the Brown particle density ρ.

IV. MAGNETIC POTENTIAL AND SWITCHING MODES

Our theory assumes a magnetic single domain for which exchange energy relevant for spatially nonuniform magnetization can be neglected, even though the effect of exchange energy enters indirectly via the Curie temperature T_C. To be specific, we will consider uniaxial anisotropy with respect to an easy axis defined along the Zeeman field $\mathbf{H} = \mathbf{H}_0 + \mathbf{H}_{\rm ac}(t)$ for which

$$\begin{aligned} \tilde{V}(m_r,\theta) &= M_s V(m_r,\theta) \\ &= -M_s(H_0 + H_{\rm ac}(t))m_r\cos\theta \\ &\quad + \frac{M_s^2}{2\chi_\perp} m_r^2 \sin^2\theta + \frac{M_s^2}{8\chi_\parallel}\left(m_r^2 - m_e^2\right)^2, \quad T \lesssim T_c, \end{aligned} \quad (14)$$

where $H_0, H_{\rm ac}(t) = H_{0\rm ac}\cos\omega t$, $\chi_\perp$, $\chi_\parallel$ are the static and alternating applied magnetic fields, both of which are along the easy axis $\hat{z}$, transverse susceptibility, and longitudinal susceptibility. respectively [38]. The m_e is a temperature-dependent $[m_e(T)]$ thermal equilibrium value of magnetization (normalized with respect to saturation magnetization) determined from solving Curie-Weiss equation

$$m_e = B_S(m_e\tilde{\beta}), \quad (15)$$

involving Brillouin function

$$B_S(m_e\tilde{\beta}) = \frac{2S+1}{2S}\coth\left(\frac{2S+1}{2S}m_e\tilde{\beta}\right) - \frac{1}{2S}\coth\left(\frac{1}{2S}m_e\tilde{\beta}\right), \quad (16)$$

where $\tilde{\beta} = S^2 J_0/(k_B T)$, S is the length of spin vector, and

$$J_0 = \frac{3k_B T_c}{S(S+1)} \quad (17)$$

is an energy scale related to Curie temperature T_C[7]. Within the framework of linear response theory and thermodynamics consideration, the coefficients in Eqs. (1)–(14) are given by [3,7]

$$\alpha_\parallel = \frac{\lambda}{m_e}\frac{2T}{3T_c}\frac{2q}{\sinh 2q}, \quad (18)$$

$$\alpha_\perp = \frac{\lambda}{m_e}\left(\frac{\tanh q}{q} - \frac{T}{3T_c}\right), \quad (19)$$

where $q = 3T_c m_e/(2(S+1)T)$. On the other hand,

$$\chi_\perp(T=0) = \frac{M_s^2}{2K(T=0)}, \quad \chi_\perp(T) = \frac{M_s^2 m_e^2(T)}{2K(T)} \quad (20)$$

is deduced from the experimental value of the anisotropy coefficient $K(T)$ while

$$\chi_\parallel = \frac{\upsilon M_s^2}{S^2 J_0}\frac{\tilde{\beta}B_S'(m_e\tilde{\beta})}{(1-\tilde{\beta}B_S'(m_e\tilde{\beta}))}, \quad (21)$$

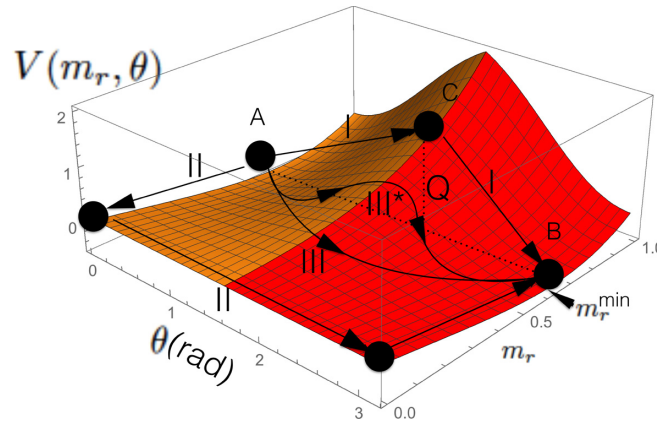

FIG. 1. The profile of the snapshot of the magnetic potential $V(m_r,\theta,t)$ in Eq. (14) at zero static field $H_0 = 0$ but finite alternating field $H_{0\rm ac} > 0$ at $t = 0 (t = \pi/\omega)$ displayed in orange (red) driving a displacement of the Brown magnetic particle between the two minima A and B across a maximum C of height Q relative to the two minima. The possible modes of magnetic switching correspond to different trajectories of Brown particle displacement: I– III correspond to the standard circular, linear, and elliptical switching modes [38]. The one labeled by III* is the nutation-driven switching mode emerging in inertial regime.

where $B_S' = dB_S(x)/dx$. Only $T \lesssim T_c$ is considered in the present paper because the application of our theory is aimed at magnetization reversal in ferromagnetic (not paramagnetic) state.

The profile of the potential is given in Fig. 1 depicting the snapshots of $V(m_r,\theta,t)$ at two different instants of time: $t = 0, \pi/\omega$. Without the static and ac fields, one obtains two lines of global minima at $\theta = 0, \pi$. A key role will be played by alternating field $H_{\rm ac}$ to excite the nutation that is the hallmark of inertial term, while noting that $H_{\rm ac}$ is directed along the easy axis rather than normal to it [12,13]. Adding the ac field, one obtains an isolated point global minimum at $m_r^{\min} = f(M_s, \chi_\parallel, m_e, H_{0\rm ac})$ when $t = 0, \pi/\omega$ where the function f is provided as follows. Given that $H_{\rm ac}(t) = H_{0\rm ac}\cos\omega t$ and taking zero static field $H_0 = 0$, the potential has an isolated global minimum at

$$\begin{aligned} m_r^{\min} &= \frac{m_e^2 M_s}{3^{\frac{1}{3}}\left(9\chi_\parallel H_{0\rm ac}M_s^2 + \sqrt{3}\sqrt{27\chi_\parallel^2 H_{0\rm ac}^2 M_s^4 - m_e^6 M_s^6}\right)^{\frac{1}{3}}} \\ &\quad + \frac{\left(9\chi_\parallel H_{0\rm ac}M_s^2 + \sqrt{3}\sqrt{27\chi_\parallel^2 H_{0\rm ac}^2 M_s^4 - m_e^6 M_s^6}\right)^{\frac{1}{3}}}{3^{\frac{2}{3}} M_s}, \end{aligned} \quad (22)$$

where the right-hand side of the equation defines the function $f(M_s, \chi_\parallel, m_e, H_{0\rm ac})$ mentioned earlier. The effective field due to the potential V is given by

$$\mathbf{F} = -\frac{\delta V}{\delta \mathbf{m}} = (H_0 + H_{\rm ac}(t))\hat{z} - \frac{M_x\hat{x} + M_y\hat{y}}{\chi_\perp} + \frac{\left(1 - \frac{m_r^2}{m_e^2}\right)}{2\chi_\parallel}\mathbf{M} \quad (23)$$

in Cartesian coordinates for easier visualization. It can be seen that it is the anisotropic field that induces a precessional

TABLE I. Comparison of basic parameters and dynamical magnetic properties of gadolinium (Gd), a rare-earth metal (lanthanide, more precisely), and several most common transition metal ferromagnets. Operating temperature $T = 280$ K and $H_{0\mathrm{ac}} = 0.5$ T (for $m_r^{\min}$).

Quantity	Gadolinium (Gd)	Iron (Fe)	Nickel (Ni)	Cobalt (Co)
Curie temperature T_C (Kelvin)	293	1043	627	1388
Effective spin S	3.5 [44]	1.5 [45]	1 [45]	2 [45]
Exchange energy J_0 (Joule) [Eq. (17)]	7.7×10^{-22}	1.2×10^{-21}	4.5×10^{-21}	5.2×10^{-21}
Uniaxial anisotropy constant $K(T)$ (Jm^{-3})	2.5×10^4 [44,46]	4.9×10^4 [47]	2.9×10^3 [48]	5.5×10^5 [49,50]
Saturation magnetization M_s (Joule $\mathrm{Tesla}^{-1}\mathrm{m}^{-3}$)	2.5×10^5 [51]	1.7×10^6 [52]	4.9×10^5 [52]	1.4×10^6 [53]
Dimensionless equilibrium magnetization $m_e(T)$ [Eqs. (15) and (16)]	0.300	0.992	0.958	0.995
Dimensionless V-minimizing magnetization $m_r^{\min}$ [Eq. (22)]	0.374	0.992	0.958	0.995
Magnetic system volume v(in units of $10^{-30}\mathrm{m}^3$)	66.2	23.6	15.2	21.8
Transverse damping coefficient $\alpha_\perp$ [Eq. (19)]	0.2259	0.0354	0.0443	0.0334
Thermal diffusion coefficient k' (s^{-1}) [Eq. (4)]	9.15×10^{12}	5.96×10^{11}	4.03×10^{12}	7.43×10^{11}
Longitudinal damping coefficient $\alpha_\parallel$ [Eq. (18)]	0.2108	0.0019	0.0080	0.0010
Ratio $\alpha_\parallel/\alpha_\perp$	0.9331	0.0537	0.1809	0.0288
Transverse susceptibility $\chi_\perp(T)$ (Joule $\mathrm{Tesla}^{-2}\mathrm{m}^{-3}$) [Eq. (20)]	1.16×10^5	2.95×10^7	3.88×10^7	1.76×10^6
Longitudinal susceptibility $\chi_\parallel(T)$ (Joule $\mathrm{Tesla}^{-2}\mathrm{m}^{-3}$) [Eq. (21)]	4709.13	100.27	47.57	20.64
Error factor δ [Eq. (8)]	0.2676	0.0013	0.0021	0.0011

motion that will drive a reversal of magnetization between the two minima along $\pm\hat{z}$.

Figure 1 visualizes an energy landscape with two minima separated by a barrier of height $Q \simeq vK$. The tunneling between these two minima corresponds to magnetic switching between two opposite magnetization orientations. Paths on the energy landscape corresponding to the different modes of magnetization reversal are also shown in Fig. 1. Standard modes for magnetization reversal consist of circular (Stoner-Wolfrath) switching at low temperature limit (I), elliptical switching at moderate temperatures (III), and linear switching at high temperatures, near Curie temperature (II). The prospective magnetic switching mode in the inertial regime involves nutation, labeled by III* in Fig. 1. The existence of two minima at $\theta = 0, \pi$ requires $H_{0\mathrm{ac}} > H_0$, permitting magnetic switching type III* to occur even in the absence of static field.

The magnetic transverse damping coefficient $\alpha_\perp$ in Eq. (19) and the V-minimizing magnetization $m_r^{\min}$ in Eq. (22) give rise to a field-temperature ($H_{0\mathrm{ac}} - T$) parameter space with varying size of error factor δ that determines the accuracy of our approximation, as discussed in Sec. III. We will illustrate and apply our theory to some familiar ferromagnetic metals: gadolinium (Gd); a rare-earth metal (lanthanide, more precisely) and several most common transition-metal ferromagnets; iron (Fe), nickel (Ni), and cobalt (Co) with basic parameters presented in Table I for comparison. The error factor $\delta(H_{0\mathrm{ac}}, T)$ is presented in the form of color contour plots for the four elemental ferromagnets considered as examples in this paper in Fig. 2. The four subfigures indicate that for Fe, Ni, and Co, the error factor is reasonably small that our approximation $1 + \alpha_\perp^2/m^2 \simeq 1$ is justified everywhere near room temperature. On the other hand, for Gd, a small enough error factor requires working at relatively cold temperatures and strong ac field. Figure 2 can thus be used as reference map for the region of applicability or degree of accuracy of our theory.

In addition, it can be seen that the error factors of the three ferromagnetic transition metal elements (Fe, Ni, and Co) are practically independent of the amplitudes of ac field $H_{0\mathrm{ac}}$ while varying with the operating temperature T like a temperature gradient. This is because for these three elements, the near-room temperatures are relatively low with respect to their Curie temperature, T_C. It can be verified from Eq. (21) that $\chi_\parallel \to 0$ as $T \to 0$. The dependence of error factor on $H_{0\mathrm{ac}}$ only enters via the potential energy-minimizing magnetization $m_r^{\min}$ and it can be checked from Eq. (22) that $m_r^{\min} \to m_e$

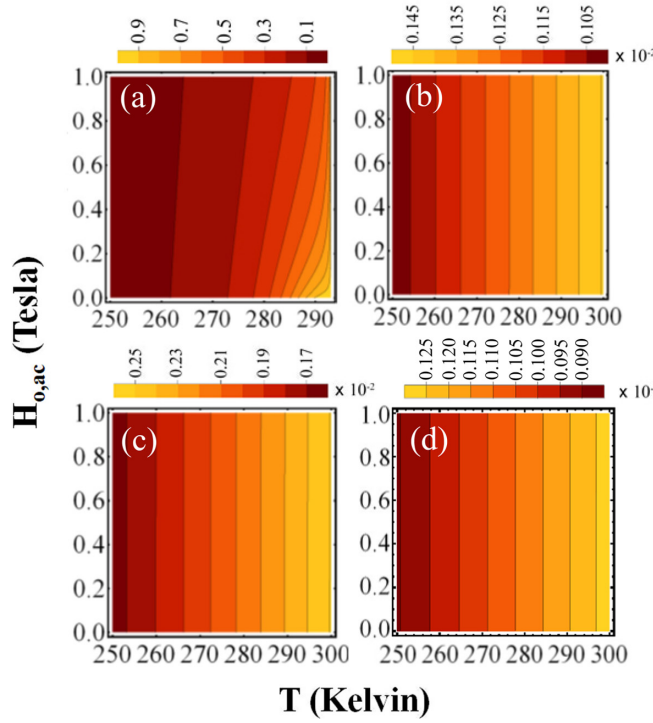

FIG. 2. The color contour plots of the error factor $\delta(H_{0\mathrm{ac}}, T)$ for the four elemental ferromagnets under consideration (a) Gd, (b) Fe, (c) Ni, and (d) Co. The darker the region, the lower the error introduced by our approximation: $1 + \alpha_\perp^2/m^2 \simeq 1$.

as $\chi_\parallel \to 0$ when $T \to 0$ or $T \ll T_c$, noting also that $m_e(T = 0) = 1.0$. As such, the potential energy-minimizing magnetization $m_r^{\min}$ and the error factor are practically independent of $H_{0\mathrm{ac}}$ (though still weakly varying on T) at temperatures much lower than T_C. For Gd, on the other hand, the color contour plot of the error factor displays more variation and also a nonlinear feature on the high temperature side. This is because the operating temperature T already approaches the Curie temperature $T_C = 293$ K, making the $m_r^{\min}$ and error factor strongly dependent on both $H_{0\mathrm{ac}}$ and T near T_C. In this paper, we will work at a specified operating temperature $T = 280$ K and ac field $H_{0\mathrm{ac}} = 0.5$ Tesla to give concrete results; the temperature at 280 K is chosen because it is reasonably close to room temperature, even though a tolerance for about 27% error factor for Gd is implied (Table I), while the error factor is much smaller for Fe, Ni, and Co at this operating temperature. However, our paper gives all the necessary details that permit the readers to repeat the calculation for any arbitrary values of $H_{0\mathrm{ac}}$ and $T < T_C$.

V. SOLUTION OF FOKKER-PLANCK EQUATION

The speed of various switching modes considered above is to be computed from the escape rate of the Brownian particle by first solving the Fokker-Planck Eq. (13). Considering that the system still has axial symmetry, we solve the Fokker-Planck equation using the ansatz

$$\rho(m_r, \theta, t) = \rho_0(m_r, \theta) + \delta\rho(m_r, \theta, t), \tag{24}$$

with explicit dependence on m_r. The zeroth order solution for particle density can be determined by considering the steady-state situation $\partial\rho/\partial t = 0$ in Eq. (13), subject to the actual potential energy Eq. (14). It can be checked that the stationary-state solution corresponding to statistical equilibrium can only be achieved if we turn off the alternating magnetic field, that is, $H_{\mathrm{ac}} = 0$. In such statistical equilibrium, the particle density should in principle take the form

$$\rho_0(m_r, \theta, t) = \rho_0(m_r, \theta) \sim e^{-\frac{v\tilde{V}(m_r,\theta)}{k_B T}}. \tag{25}$$

The task is to find the proportionality function, which in this case is not necessarily constant (normally taken to be unity). To that end, it is helpful to work with the continuity equation in the original form from Eq. (13),

$$\frac{\frac{\partial}{\partial m_r}\left(m_r^2 J_r\right)}{m_r^2} + \frac{\frac{\partial}{\partial\theta}(\sin\theta J_\theta)}{m_r \sin\theta} = 0, \tag{26}$$

where we have set $\partial\rho/\partial t = 0$ and used the fact that the J_ϕ has no dependence on ϕ at all. Clearly, the equation is satisfied by a ρ_0 such that $J_r = J_\theta = 0$. So, using Eqs. (10) and (11), we have

$$-\rho\gamma_0\alpha_\parallel \frac{\partial V}{\partial m_r} - k' \frac{\partial\rho}{\partial m_r} = 0, \tag{27}$$

$$-\rho \frac{\alpha_\perp \gamma_0}{m_r} \frac{\partial V}{\partial\theta} - \frac{k'}{m_r} \frac{\partial\rho}{\partial\theta} = 0 \tag{28}$$

to be solved for ρ, that gives ρ_0. Solving Eq. (28) first immediately gives

$$\rho_0(m_r, \theta) = A_0(m_r) e^{-\frac{v\tilde{V}(m_r,\theta)}{k_B T}}, \tag{29}$$

where we have used the definition of k' as given in Eq. (4). Then, substituting Eq. (29) into Eq. (27), we obtain

$$A_0(m_r) = D_0 e^{(1-\frac{\alpha_\parallel}{\alpha_\perp})\frac{v\tilde{V}_s(m_r)}{k_B T}}, \tag{30}$$

where $\tilde{V}_s(m_r)$ refers to the θ-independent part of $\tilde{V}(m_r, \theta)$, thus corresponding to the longitudinal relaxation part in our model. The full solution for the stationary-state density is thus given by

$$\rho_0(m_r, \theta) = D_0 e^{(1-\frac{\alpha_\parallel}{\alpha_\perp})\frac{v\tilde{V}_s(m_r)}{k_B T}} e^{-\frac{v\tilde{V}_s(m_r,\theta)}{k_B T}}, \tag{31}$$

where $\tilde{V}_s(m_r), \tilde{V}_s(m_r, \theta)$ are, respectively, the $\theta + t$-independent and t-independent parts of Eq. (14) while $D_0 > 0$ is a reference value for the particle density. As can be seen in Table I, one indeed has $\alpha_\parallel \simeq \alpha_\perp$ for certain elemental ferromagnets when working at operating temperature $T \lesssim T_C$ such as gadolinium (Gd) at $T = 280$ K; the steady state solution Eq. (31) therefore then takes a Boltzmann distribution in terms of the potential energy $V(m_r, \theta)$ in Eq. (14) as required for statistical equilibrium. On the other hand, as can be seen from Table I, this condition $\alpha_\perp \simeq \alpha_\parallel$ is not satisfied by transition-metal ferromagnets iron, nickel, and cobalt at $T = 280$ K. Nevertheless, at much higher temperatures close to their respective Curie temperature $T \lesssim T_C$, it can be verified using Eqs. (18) and (19) that the condition $\alpha_\perp \simeq \alpha_\parallel$ is again satisfied. However, working at $T \lesssim 627, 1043, 1388$ K is evidently not of practical interest for a spintronic device.

Based on Eq. (31), when $\alpha_\perp \simeq \alpha_\parallel$ is not satisfied, one still obtains a Boltzmann-like distribution in terms of an effective potential energy that differs from the original potential $\tilde{V}(m_r, \theta)$ in Eq. (14),

$$\begin{aligned}\tilde{V}_{\mathrm{eff}}(m_r, \theta) &= \tilde{V}_s(m_r, \theta) - \left(1 - \frac{\alpha_\parallel}{\alpha_\perp}\right)\tilde{V}_s(m_r) \\ &= -M_s H_0 m_r \cos\theta + \frac{M_s^2}{2\chi_\perp} m_r^2 \sin^2\theta \\ &\quad + \frac{\alpha_\parallel}{\alpha_\perp}\frac{M_s^2}{8\chi_\parallel}\left(m_r^2 - m_e^2\right)^2 \\ &\simeq -M_s H_0 m_r \cos\theta + \frac{M_s^2}{2\chi_\perp} m_r^2 \sin^2\theta,\end{aligned} \tag{32}$$

where the last line in Eq. (32) applies when $\alpha_\parallel \ll \alpha_\perp$, as is especially the case for Fe and Co according to Table I, resulting in an effective magnetic potential without the longitudinal fluctuation energy term, corresponding to fixed magnitude of magnetization $|\mathbf{M}|$. This latter effective potential can indeed be used as an approximate description for magnetization dynamics at an operating temperature much lower than the Curie temperature $T \ll T_C$ since in that regime the thermal fluctuations that drive the longitudinal relaxation are weak. It can be seen that our theory based on the Fokker-Planck equation provides a self-consistent description of magnetization dynamics for ferromagnets with a diverse range of Curie temperatures.

Substituting the ansatze Eq. (24) into the Fokker-Planck Eq. (13), we obtain an exact analytical solution only for the case with constant potential. The four terms in Eq. (14) will thus be treated as perturbation terms, even though only H_0 and $H_{0\mathrm{ac}}$ are tunable. The exact analytical solution for the

case with a (hypothetical) constant potential $V(m_r,\theta)=V_0$ is derived as follows. Readers interested only in the final result can skip the following derivation and jump immediately to the end of this section.

Since ferromagnets with uniaxial symmetry still have axial symmetry, the solution of the Fokker-Planck equation in terms of the magnetic charge density ρ will be independent of ϕ. Calling $x=\cos\theta, y=m_r$, we find that our Fokker-Planck Eq. (13) can be written as

$$\frac{\partial\rho(x,y,t)}{\partial t}+\mathbf{D}\cdot\boldsymbol{\nabla}\rho(x,y,t)+E[\rho(x,y,t)] = M(x,y,t)\rho(x,y,t), \tag{33}$$

where $\boldsymbol{\nabla}=(\partial/\partial x,\partial/\partial y)$ and

$$\mathbf{D}(x,y,t)=\left(-\frac{1-x^2}{y^2}\alpha_\perp\gamma_0\left(\frac{\partial V}{\partial x}+\tau\frac{\partial^2 V}{\partial x\partial t}\right),\alpha_\parallel\gamma_0\frac{\partial V}{\partial y}\right), \tag{34}$$

$$E[\rho(x,y,t)]=-\frac{k'}{y^2}\frac{\partial}{\partial y}\left(y^2\frac{\partial\rho}{\partial y}\right)-\frac{k'}{y^2}\frac{\partial}{\partial x}\left[(1-x^2)\frac{\partial\rho}{\partial x}\right] \tag{35}$$

$$M(x,y,t)=\alpha_\parallel\gamma_0\left(\frac{2}{y}\frac{\partial V}{\partial y}+\frac{\partial^2 V}{\partial y^2}\right)+\frac{\alpha_\perp\gamma_0}{y^2}\frac{\partial}{\partial x}\left[(1-x^2)\left(\frac{\partial V}{\partial x}+\tau\frac{\partial^2 V}{\partial x\partial t}\right)\right], \tag{36}$$

where

$$V(x,y,t)=-(H_0+H_{\rm ac}(t))yx+\frac{y^2}{2\chi_\perp}(1-x^2)+\frac{\left(y^2-y_e^2\right)^2}{8\chi_\parallel}. \tag{37}$$

Perturbation theory will be used by starting from the solution of our Fokker-Planck equation but assuming a constant potential energy $V=V_0$ followed by perturbation expansion in $v\tilde{V}/(k_BT)$ using methods in mathematical physics [39].

With constant potential, the full Fokker-Planck equation can be decoupled into x and y parts and written as eigenvalue problems,

$$L_x\left(u_n^x(x)\right)+\lambda_n^x u_n^x(x)=0, \tag{38}$$

$$L_y\left(u_{n\alpha}^y(y)\right)+\lambda_n^y u_{n\alpha}^y(y)=0, \tag{39}$$

where L_x, L_y are some differential operators, the detailed form of which is given in Appendix B, while $u_n^x(x), u_{n\alpha}^y(y)$ are the unperturbed eigenfunctions and $\lambda_n^x, \lambda_{n\alpha}^y$ are the corresponding eigenvalues.

With the details of derivation given in Appendix B, it is found that

$$u_n^x(x)=c_{Pn}P_n(x),\quad u_{n\alpha}^y(y)=c_{yn\alpha}\mathcal{Y}_{-n-1}(u_{-n-1,\alpha}y), \tag{40}$$

with $x=\cos\theta, y=m_r$, involving a spherical Bessel function $\mathcal{Y}_{-n-1}(y)$ of order $-n-1$, $u_{-n-1,\alpha}\simeq(n/2+\alpha+1)\pi$ is the αth zero of the $\mathcal{Y}_{-n-1}(y)$, and $P_n(x)$ is a Legendre polynomial of nth order. The eigenvalues are given by

$$\lambda_n^x=-n(n+1),\ \lambda_{n\alpha}^y=-\frac{n(n+1)}{u_{-n-1,\alpha}^2}, \tag{41}$$

corresponding, respectively, to the Legendre and spherical Bessel functions as the eigenfunctions.

Given the above results, the solution of the Fokker-Planck Eq. (33) for the unperturbed case (constant potential energy) in terms of the Brown magnetic particle density is found to be that given by Eq. (24) with

$$\delta\rho(m_r,\theta,t)=\sum_{n=1,\alpha=0}^{\infty}c_{n\alpha}u_n^x(\cos\theta)u_{n\alpha}^y(m_r)e^{-p_{n\alpha}t}. \tag{42}$$

The coefficients are determined by the initial condition $\delta\rho(x,y,0)$. The $p_{n\alpha}$ is the eigen-(damping)frequency (or eigendecay (or damping) rate more precisely),

$$p_{n\alpha}=u_{-n-1,\alpha}^2k'\simeq k'\left(\frac{n}{2}+\alpha+1\right)^2\pi^2, \tag{43}$$

indicating a decay rate that is quadratically dependent on the mode number n and is proportional to the coefficient k' that characterizes thermal fluctuation-induced diffusion of Brownian particles giving rise to an exponential temporal dependence $\exp(-p_{n\alpha}t)$.

Turning on the magnetic potential $V(m_r,\theta,t)$ in Eq. (14), the full solution for the particle density is computed perturbatively in $vM_sH_{0(0\rm ac)}/(k_BT), vM_s^2/(\chi_{\perp(\parallel)}k_BT)\ll 1$ using perturbation theory [39], where in Eq. (42) we will have $u_n^x\to\overline{u}_n^x, u_{n\alpha}^y\to\overline{u}_{n\alpha}^y, p_{n\alpha}\to\overline{p}_{n\alpha}$. In addition to the above equations, conservation of Brown particle density is implied by the continuity Eq. (5); the decay of the density at a point (corresponding to a minimum of the magnetic potential energy) in the sphere must give rise to a growth of the density at another point (corresponding to another minimum of the magnetic potential energy) on the sphere.

VI. PERTURBATIVE SOLUTION OF FOKKER-PLANCK EQUATION WITH MAGNETIC POTENTIAL $V(m_r,\theta,t)$

Perturbation theory is defined by expanding the perturbed eigenfunctions and the eigenvalues [39],

$$\overline{u}_n^x(x,y,t)=u_n^x(x)+\epsilon_x v_n^x(x,y,t)+\epsilon_x^2 w_n^x(x,y,t)+\cdots, \tag{44}$$

$$\overline{\lambda}_n^x(y)=\lambda_n^x+\epsilon_x\mu_n^x(y)+\epsilon_x^2\nu_n^x(y)+\cdots, \tag{45}$$

$$\overline{u}_{n\alpha}^y(x,y,t)=u_{n\alpha}^y(y)+\epsilon_y v_{n\alpha}^y(x,y,t)+\epsilon_y^2 w_{n\alpha}^y(x,y,t)+\cdots, \tag{46}$$

$$\overline{\lambda}_{n\alpha}^y(x)=\lambda_{n\alpha}^y+\epsilon_y\mu_{n\alpha}^y(x)+\epsilon_y^2\nu_{n\alpha}^y(x)+\cdots, \tag{47}$$

where the unperturbed eigenfunctions $u_n^x(x), u_{n\alpha}^y(y)$ and unperturbed eigenvalues $\lambda_n^x, \lambda_{n\alpha}^y$ are those given in the previous section. We will eventually work only up to first-order corrections in the eigenfunctions and eigenvalues justified by the fact that $\epsilon_x,\epsilon_y\sim vM_sH_0/(k_BT), vM_sH_{0\rm ac}/(k_BT)\ll 1$ and as well $vM_s^2/(\chi_\perp k_BT), vM_s^2/(\chi_\parallel k_BT)\ll 1$ for the system of our interest. It is to be noted that the expansion is slightly more complicated than that for single-variable perturbation theory because we now have two independent variables x and y, resulting in perturbed eigenfunctions that are now in general functions of both x and y and perturbed eigenvalues that are also functions of one of the two variables x or y. The task is

TABLE II. Comparison of expansion parameters (EPs) in our perturbation solution of the Fokker-Planck equation applied to gadolinium (Gd), a rare-earth metal (lanthanide, more precisely), and several most common transition metal ferromagnets. The value within parentheses is the longitudinal susceptibility expansion parameter multiplied by the scaling factor $\alpha_\parallel/\alpha_\perp$ of the effective potential in Eq. (32). Operating temperature $T = 280$ K and $H_{0\mathrm{ac}} = 0.5$ T.

Perturbation expansion parameter	Gadolinium (Gd)	Iron (Fe)	Nickel (Ni)	Cobalt (Co)
Transverse susceptibility EP $\epsilon^{\chi_\perp} = \frac{vM_s^2}{\chi_\perp k_B T}$	0.009499	0.000607	0.000024	0.006282
Longitudinal susceptibility EP $\epsilon^{\chi_\parallel} = \frac{vM_s^2}{\chi_\parallel k_B T}((\frac{\alpha_\parallel}{\alpha_\perp})\epsilon^{\chi_\parallel})$	0.233(0.217)	178.471(9.577)	20.012(3.617)	540.787(15.499)
ac field EP $\epsilon^{H_{0\mathrm{ac}}} = \frac{vM_sH_{0\mathrm{ac}}}{k_B T}$	0.002172	0.005222	0.000968	0.003957

to compute the perturbation expansion functions appearing in Eqs. (44)–(47), the details of which are given in Appendix C.

Before proceeding with the calculation of the coefficients of the perturbation expansion, we evaluate the perturbation expansion parameters of the elemental ferromagnets as considered in Table I. Their numerical values are presented in Table II. As can be seen, at the near-room temperature of interest $T = 280$ K, the perturbation expansion parameters are all smaller than unity for Gd, but those of Fe, Ni, and Co exceed unity for longitudinal relaxation energy terms, even after scaled by the corresponding factor $\alpha_\parallel/\alpha_\perp$. This suggests that our perturbation theory breaks down and is not applicable to the latter three elements, at least at the temperature $T = 280$ K of interest, which is relatively low compared to the Curie temperatures of the three transition metal ferromagnets. There are two possible options to remediate this problem. First, the longitudinal relaxation term is dropped altogether, justified by taking the $\alpha_\parallel/\alpha_\perp \to 0$ approximation in the effective magnetic potential $\tilde{V}_{\mathrm{eff}}(m_r, \theta)$ in Eq. (32), thus the longitudinal relaxation term is no longer present in the perturbation theory. Second, the iLLGB equation of motion is solved fully numerically rather than analytically using our perturbation theory. Certainly, one may consider a much higher operating temperature T closer to the respective T_C of each of the transition metal ferromagnets but, as mentioned in the previous section, this is not of practical interest for near-room temperature spintronic applications. The implication of the breakdown of perturbation theory on the final result in terms of the magnetization reversal rate will be discussed in the next section.

VII. MAGNETIZATION REVERSAL RATE

From previous analysis, the dynamics has two sources of time dependence; one due to the exponential decay with time, reflecting the diffusion of the Brownian particle driven by the thermal fluctuations, the other due to the driving field $H_{\mathrm{ac}}(t)$ hiding in the perturbed eigenfunctions, also containing inertial effect. These two are to be referred to as, respectively, exponential mode and nutation mode. The exponential mode is nothing but the thermal switching corresponding to superparamagnetism, the speed of which is directly estimable using Eqs. (4) and (43), giving a characteristic switching rate

$$R^{\mathrm{switching}}_{\mathrm{thermal-diffusion}} \simeq \frac{9}{4}\pi^2 \frac{k_B T}{v} \frac{\alpha_\perp \gamma_0}{M_s}\left[1 - O_1\left(\frac{v\tilde{V}}{k_B T}\right)\right] \quad (48)$$

taken from the eigendecay rate with $n = 1, \alpha = 0$, which turns out to be proportional to the system temperature, but inversely proportional to the saturation magnetization, a very intuitive result because a magnetization vector of smaller magnitude can reverse faster. This superparamagnetic mode, however, does not lead to a stable magnetic switching because the Brown particle keeps moving between the two minima.

The switching rate in the field-dominated region can be determined by looking at Fig. 1. If the Brown particle is swept along the topography of the $V(m_r, \theta, t)$ in such a way that it always sticks to the locus of the minimum of $V(m_r, \theta, t)$ at any t, then one has

$$R^{\mathrm{switching}}_{\mathrm{field}} = 2\nu\left[1 - O_2\left(\frac{v\tilde{V}}{k_B T}\right)\right], \quad (49)$$

where $\nu = \omega/(2\pi)$ is the frequency of the ac field, 2ν being an upper bound on the field-driven switching rate. Our perturbation theory calculation does not give simple analytical expressions for the correction terms $0 < O_{1,2}(v\tilde{V}/(k_B T)) \ll 1$ in terms of all pertinent parameters. The perturbative corrections $O_{1,2}(v\tilde{V}/(k_B T))$ are small when the argument $v\tilde{V}/(k_B T)$ is small, but can be significant and thus significantly reduces the corresponding switching rate when $v\tilde{V}/(k_B T)$ is rather large.

As an illustration, the theory is applied to magnetization dynamics in a ferromagnetic element with Curie temperature near room temperature: gadolinium (Gd). The resulting profile of $\rho(m_r = 0.5, x = \cos\theta, t)$ is shown in Fig. 3 where the following numerical values for the parameters have been used [44,46,51] as also summarized in Table I: $T_C = 293$ K, $T = 280$ K, $J_0 = 7.7 \times 10^{-22}$ J, M_s=2.54×10^5 J Tesla^{-1}m^{-3}, $m_e(T) = 0.3$, $m_r^{\mathrm{min}} = 0.373$, $S = 7/2$, $v = 6.62 \times 10^{-29}$ m^3, $\lambda = 0.1$, $\alpha_\perp = 0.226$, $\alpha_\parallel = 0.211$, $\chi_\parallel = 4.71 \times 10^3$ J Tesla^{-2} m^{-3}, $\chi_\perp = 1.16 \times 10^5$ J Tesla^{-2} m^{-3}, $k' = 9.15244 \times 10^{12}$ s^{-1}, $H_0 = 0.0$ Tesla, $H_{0\mathrm{ac}} = 0.5$ Tesla, $\tau = 10^{-11}$s, $\omega = 2\pi/T_{\mathrm{period}}$, $T_{\mathrm{period}} = 10^{-14}$s, $D_0 = 1$/unitcell whereas the standard constants are $k_B = 1.38 \times 10^{-23}$ m^2 kgs^{-2}K^{-1}, $\gamma_0 = 1.76 \times 10^{11}$ C kg^{-1}, $\mu_B = 9.274 \times 10^{-24}$ J Tesla^{-1} for the Boltzmann factor, gyromagnetic ratio, and Bohr magneton, respectively. Substituting the above parameters, we obtain $R^{\mathrm{switching}}_{\mathrm{thermal-diffusion}} = 2.0 \times 10^{14}$ s^{-1}, corresponding to subpicosecond switching time already; $\tau^{\mathrm{switching}}_{\mathrm{thermal}} = 1/R^{\mathrm{switching}}_{\mathrm{thermal-diffusion}} = 0.5 \times 10^{-14}$ s. On the other hand, for the field-driven nutation mode, the switching time is half the period of the ac field; $\tau^{\mathrm{switching}}_{\mathrm{field}} = 0.5 \times 10^{-14}$ s.

The switching time can be estimated from the time evolution of the Brown particle density, more precisely in terms of its change from statistical equilibrium value $\delta\rho(x, y, t) \equiv \delta\rho(m_r, \theta, t)$. A particularly simple initial condition is given

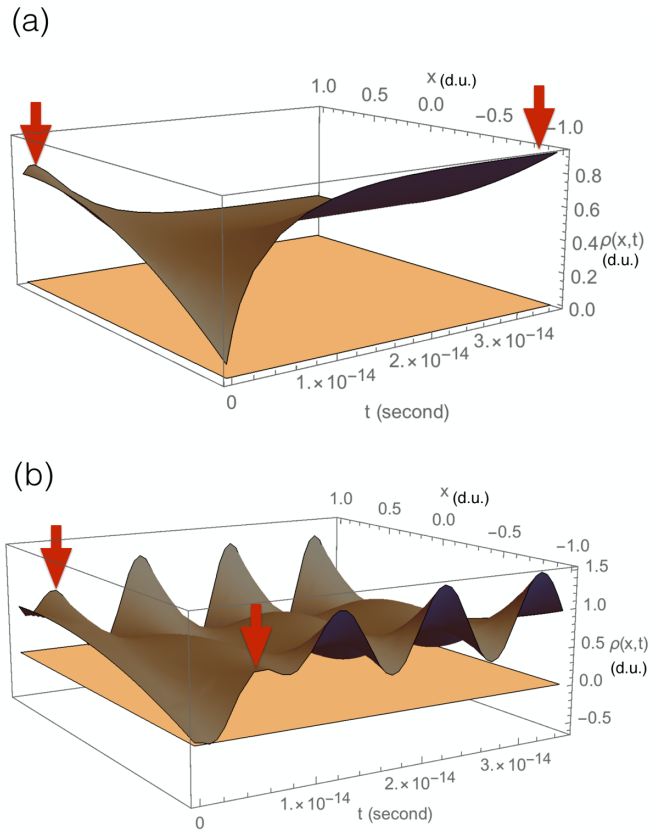

FIG. 3. The time-space evolution of Brown particle density $\rho(m_r = 0.5, x = \cos\theta, t)$: (a) without static and ac fields applied; (b) with $H_0 = 0$ and $H_{0\mathrm{ac}} = 0.5$ Tesla. The parameters used are given in Table I and the text. Red arrows mark time periods corresponding to complete magnetization reversals.

by

$$\delta\rho(m_r, \theta, t = 0) = \delta\rho_0 + D_0\left(\sum_{n=0}^{\infty} \eta_n \cos^n\theta\right) e^{\left(1-\frac{\alpha_\parallel}{\alpha_\perp}\right)\frac{v\bar{V}_s(m_r)}{k_B T}}, \tag{50}$$

subject to a constraint $\eta_{n+1} \ll \eta_n \ll \cdots \ll \eta_1 \leqslant 1$, assuming that the static fields (including the anisotropy and longitudinal relaxation fields) are applied at $t = 0^+$. This initial condition has been used to produce Fig. 3. The $\delta\rho_0$ is a constant chosen in such a way that $\rho(m_r, \theta = 0, 0) = \tilde{\rho}_0 > \rho_0$ while $\rho(m_r, \theta = \pi, 0) = 0$, where ρ_0 is given by Eq. (31) at $V_s = 0$, a second constraint designed to describe Brown particles initially accumulating in the northern hemisphere near the north pole. In producing Fig. 3, we have used the same $\delta\rho_0 = 0$, $\eta_0 = -0.36$, $\eta_1 = 1.0$, $\eta_2 = 0.6$, and the sum is taken over a few first modes $n = 0, 1, 2$, because eventually only these three modes are generated with the above choice of initial condition, for both parts of the figure. The reason we add the η_0 is to generate a strong $v_1^{H_{\mathrm{ac}},x}(x, y, t)$ term in the perturbation expansion Eq. (44) which would give a strong switching effect since it is odd in x. The presence of nonzero η_0 means a breathing mode contribution; that is, an isotropic perturbation of the distribution of Brown particles from thermal equilibrium distribution. This isotropic component is dominant when the anisotropy energy is small. Experimentally, anisotropy coefficient $K(T)$ decreases as one increases the temperature T from below T_C [44,47]. This means, as long as one works at high enough temperatures (but lower than T_C), the anisotropy energy is small and the system tends to have isotropic nonequilibrium distribution of magnetization orientation. The initial condition assumed with nonzero η_0 is thus a pertinent rather than an *ad hoc* or artificial assumption, and thus corresponds to realistic experimental situations, as long as one operates at high enough temperatures (below T_C) in such a way that the anisotropy energy is smaller than the energy scales that drive the switching (thermal energy and especially the driving field energy). The switching effect predicted in this paper is thus realistic to be manifested in experiment, under the above condition. In applying our theory, however, the operating temperature T should not be too close to T_C to not augment the error factor δ [Eq. (8)] associated with the approximation $1 + \alpha_\perp^2/m^2 \simeq 1$.

The switching time is estimated from the sum of the decay time of the Brown particle density at $\theta = 0$ and the growth time of the same quantity at $\theta = \pi$. The results are compared with $\tau = 0$ (adiabatic switching) and nonzero τ, for which inertial switching occurs for timescales smaller than τ. Imposing the conservation of the number of Brown particles, it can be shown that in the thermal diffusion-dominated region, the Brown particle density can be simplified to (in terms of $x = \cos\theta$, $y = m_r$)

$$\begin{aligned}\rho(x, y = y_0, t) &= \delta\rho_0 + \frac{\rho_0}{2} + \sum_{n=1}^{\infty} \delta\rho_n(x)\left(e^{-p_n t} - \frac{1}{2}\right) \\ &\simeq \delta\rho_0 + \frac{\rho_0}{2} + \tilde{\rho}_0 x\left(e^{-p_1 t} - \frac{1}{2}\right),\end{aligned} \tag{51}$$

where $\tilde{\rho}_0 = \sum_{n=1}^{\infty} \delta\rho_n(x)$ at a fixed value of $y = y_0$, while the last line of Eq. (51) is for a single mode ($n = 1$) approximation. In the presence of ac field, the time dependence contains a sinusoidal term. The $\delta\rho_0$ is chosen in such a way that makes sure $\rho(x, y, t)$ is non-negative everywhere.

Figure 3(a) illustrates the time evolution of the Brown particle density in the presence of thermal diffusion (k'), uniaxial anisotropy ($\chi_\perp$), and longitudinal relaxation ($\chi_\parallel$) in the absence of static and ac fields. Switching occurs corresponding to mode III in Fig. 1, which is entirely thermally dominated, with switching time that is nevertheless subpicosecond. Figure 3(b) demonstrates the effect of static and ac fields, showing that sinusoidal external force can produce an even shorter switching time; switching may occur when a peak in the $x < 0$ regime (southern hemisphere) spikes up while a dip occurs in the $x > 0$ regime (northern hemisphere). This corresponds to mode III* of the magnetization reversal predicted in Fig. 1. Setting $\tau \ll T_{\mathrm{period}}$ or dropping altogether the inertial term in Eq. (1), the nutational mode III* also disappears. It is clear from Fig. 3(b) that switching occurs at about $T_{\mathrm{period}}/2$. From our numerical experiments, this field-driven switching requires strong enough $H_{0\mathrm{ac}}$; the minimum required value of $H_{0\mathrm{ac}}$ is smaller for the lower temperatures, according to perturbation theory.

Our result thus suggests that within the inertial regime, a new switching mode tied to nutation emerges and only requires the presence of an alternating field. While in the

precession and Bloch terms of Eq. (1) the effect of $H_{\rm ac}(t)$ is overrun by the superparamagnetic thermal fluctuations, $H_{\rm ac}(t)$ still takes effect indirectly via inertial term and has an effective magnitude of $(\tau/T_{\rm period})H_{\rm ac}(t)$. The type-II switching, on the other hand, tends to be driven by the Bloch term in Eq. (1) but is dominated by the inertial term that gives type III* above. The type-II mode may prevail close enough to Curie temperature, induced by heating, and in the absence of ac field, but requires an appropriate modeling of temperature dependence of $|\mathbf{m}(T)|$ [7]. Finally, the type-I mode is absent (or was not observed) because it requires application of a static field and normally occurs in the low-temperature regime.

For comparison, we have computed the thermal-driven switching rate $R^{\rm switching}_{\rm thermal-diffusion}$ for common transition metal ferromagnets, presented in Table III. Taking into account the error introduced by the approximation $1+\alpha_\perp^2/m_r^2 \sim 1$ with a measure of error given by δ in Eq. (8), the error factor-corrected thermal switching rate is simply given by

$$\tilde{R}^{\rm switching}_{\rm thermal-diffusion} = (1-\delta)R^{\rm switching}_{\rm thermal-diffusion}, \tag{52}$$

where $R^{\rm switching}_{\rm thermal-diffusion}$ is given in Eq. (48). This result, however, implicitly assumes that the perturbation theory converges, giving finite value for $O_{1,2}(v\tilde{V}/(k_BT))$ small compared to unity. As discussed in the previous section, this is not the case for Fe, Ni, and Co at $T = 280\,\mathrm{K}$—relatively low compared to their Curie temperatures. A naive consequence of this is that, if we insist on relying on the result of our perturbation theory, the actual thermal diffusion-driven magnetization reversal rate of Fe, Ni, and Co would be significantly lower than the theoretically predicted values given in Table III. This is entirely in agreement with the intuitive expectation that since $T = 280\,\mathrm{K}$ is relatively low compared to T_C of these three transition metal ferromagnets, thermal fluctuations are weak and, as a consequence, the resulting thermal diffusion-driven switching rate should also be relatively low. Overall, the theoretical part of Table III suggests that gadolinium gives the highest thermal diffusion-driven magnetization reversal rate at a given temperature ($T = 280\,\mathrm{K}$). With the same argument, Eq. (49) suggests that gadolinium should also give the highest field-driven switching rate due to the fact that the perturbation expansion parameter $v\tilde{V}/(k_BT)$ is smaller for Gd than those of the three transition metal ferromagnets. The corresponding error factor-corrected field-driven switching rate is

$$\tilde{R}^{\rm switching}_{\rm field} = (1-\delta)R^{\rm switching}_{\rm field}, \tag{53}$$

where $R^{\rm switching}_{\rm field}$ is given in Eq. (49).

Our theoretical values for the switching rates (times) should, however, be taken as upper (lower) bounds to experimental values. In addition, in comparing the theoretical results and experimental data, care must be taken with respect to the operating temperature T and fields H_0 and $H_{0\rm ac}$. Higher temperatures, in general, give rise to higher thermal-driven switching rates (shorter switching times). Furthermore, the switching rates and times for compounds or alloys of compounds are not simply related to those of the constituent elements. This is because in alloys, the atoms of the constituent elements may form sublattices with nontrivial, e.g., antiferromagnetic exchange interaction between the moments at two different sublattices. Ultrafast magnetization dynamics in such a multisublattice system may require a more sophisticated theoretical description [33]. In certain situations, however, the magnetization dynamics of the different sublattices in a compound or alloy of compounds may be decoupled and, in such a case, the magnetic moment dynamics of different types of atoms may be treated independently.

Table III presents experimental data for the timescale for demagnetization, magnetization reversal (switching), and thermal-driven switching processes. It is first to be noted that our theory proposes a magnetization reversal mechanism based entirely on the transfer of angular momentum between the source of effective field (e.g., the photon or optical magnetic field via the torque applied by effective field) and the magnetic moments constituting the magnetization field. In actual experiments, however, various other mechanisms may play a role, such as electron-spin coupling, spin-lattice coupling, and electron-magnon scattering, that may contribute to the demagnetization or magnetization reversal process. Numerical data from experiments at their face values should therefore not be compared strictly quantitatively with our theoretical numbers.

Experimental data for thermal effect are available mostly in terms of thermal-assisted demagnetization time $\tau^{\rm demag}$; that is, the time taken for magnetization to decrease as the magnetic sample is heated (due to laser irradiation), approaching its Curie temperature T_C. In our framework, such a thermally assisted demagnetization process as reported in Ref. [20] manifests half of the trajectory of type-II switching illustrated in Fig. 1. The speed of such a demagnetization process depends on the precise mechanism of thermalization; how the spins have their temperature increased. Noting that experimental data demonstrate femtosecond scale for demagnetization time $\tau^{\rm demag}$, the demagnetization may, in fact, be driven by the transfer of angular momentum between the spins themselves, mediated by exchange interaction, which is a quantum spin-spin interaction. In such scenario, $\tau^{\rm demag}$ will scale as $\tau^{\rm demag} \sim 1/T_c$ under exactly the same experimental condition. This would explain, for example, the experimental data listed in the lower half of Table III for the $\tau^{\rm demag}$ of Fe and Gd in Ref. [31], which reported $\tau^{\rm demag}_{\rm Gd}/\tau^{\rm demag}_{\rm Fe} \approx 4$, differs by less than 12.5% from $T_C^{\rm Fe}/T_C^{\rm Gd} \simeq 3.56$. The finding that Gd and Tb have very close thermal-assisted demagnetization times as reported in Ref. [32] also agrees with our simple scaling picture above, noting the similar Curie temperatures ($T_C = 293(300)\,\mathrm{K}$ for Gd (Tb) respectively), giving $\tau^{\rm demag}_{\rm Gd}/\tau^{\rm demag}_{\rm Tb} \simeq 1.02 \simeq T_C^{\rm Tb}/T_C^{\rm Gd} \simeq 1.02$. It is to be noted that the thermal demagnetization time $\tau^{\rm DeMag}$ is to be distinguished from the thermal switching time that we discuss, as the latter pertains to superparamagnetism rather than the reduction of magnetization.

With regard to experimental results on field-driven magnetization reversal, a global conclusion that can be drawn from the experimental data is that the observed switching rates all satisfy the condition of being lower than the upper bound 2ν found in our theory Eq. (49). This offers a possible explanation for how the switching time could cover a relatively wide range of different scales, from few hundreds of fs to few hundreds of ps, a startling phenomenon that has been a fundamental question in ultrafast magnetism; the switching time scale is only constrained by a lower bound in fs range. Fur-

TABLE III. Comparison of theoretically predicted thermal diffusion-driven and field-driven switching rates and times in Gd, Fe, Ni, and Co and the available experimental data. Operating temperature $T = 280$ Kelvin is assumed for theoretical results. The laser frequency ν is deduced from the photon energy E_{photon} or laser wavelength λ: $\nu = E_{\text{photon}}/h = c/\lambda$, where h is the Planck constant while c is the speed of light. When not stated as nanoparticles, thin film or layer geometry is implied. (*) The nanosecond thermal switching timescale can be reproduced by our theory [Eq. (48)] using volume v of nm^3 scale corresponding to experiments instead of Å^3 we used to produce the theoretical values at the top of this table.

Theoretical results

Quantity	Gadolinium (Gd)	Iron (Fe)	Nickel (Ni)	Cobalt (Co)
Thermal switching rate $R^{\text{switching}}_{\text{thermal}-\text{diffusion}}(\text{s}^{-1})$ [Eq. (48)]	2.035×10^{14}	1.324×10^{13}	8.945×10^{13}	1.645×10^{13}
Thermal switching time $\tau^{\text{switching}}_{\text{thermal}} = 1/R^{\text{switching}}_{\text{thermal}-\text{diffusion}}(\text{fs})$	$= 4.92$	75.53	11.16	60.61
Corrected rate $\tilde{R}^{\text{switching}}_{\text{thermal}-\text{diffusion}}(\text{s}^{-1})$ [Eq. (52)]	1.489×10^{14}	1.322×10^{13}	8.926×10^{13}	1.643×10^{13}
Corrected time $\tilde{\tau}^{\text{switching}}_{\text{thermal}} = 1/\tilde{R}^{\text{switching}}_{\text{thermal}-\text{diffusion}}$ (fs)	6.72	75.63	11.19	60.68

Experimental data

Material	Thermal demagnetization time τ^{demag}	Field-driven switching time $\tau^{\text{switching}}_{\text{field}}$	Thermal switching time $\tau^{\text{switching}}_{\text{thermal}}$	Experimental details (Note: MRev: magnetization reversal, demag: demagnetization, MRecov: magnetization recovery)
Ni [20]	100 to 200 fs	–	–	60 fs $\nu = 483.54$ THz linearly polarized laser pulse, $T = 340 - 580$K, demag
Ni [21]	(230±30)fs	–	–	150 fs $\nu = 374.74$ THz linearly polarized laser pulse, $T = 300$ K, demag
Ni [22]	500 to 1000 fs	–	–	70 fs $\nu = 411$ THz laser pulse, $T = 300$ K, demag
Ni [24]	(300±70)fs(A), (3.2 ± 0.2)ps(B)	–	–	85 fs $\nu = 362.69$ THz laser pulse, $T = 300$ K, A: demag, B: MRecov
Co [27]	300 fs	–	–	50 fs $\nu = 374.74$ THz laser pulse, demag
Fe(A) [31], Gd(B) [31]	(100±25)fs(A), (430±100)fs(B)	–	–	60 fs $\nu = 374.79$ THz linearly polarized laser, $T = 83$ K
Gd(A) [32], Tb(B) [32]	(760±250)fs(A), (740±250)fs(B)	–	–	50 fs 362.69 THz circularly polarized laser pulse, $H_0 = 0.5$Tesla, $T = 140$ K, demag
GdFeCo [23]	–	$\tau^{\text{switching}}_{\text{field}} = (190 \pm 40)$ ps	–	100 fs $\nu = 374.74$ THz circularly polarized laser pulse, $T = 300$ K, $T_C = 532$ K, all-optical, MRev
DyFeO3 [25]	–	$\tau^{\text{switching}}_{\text{field}} = 2.3$ ps (resonance period)	–	200 fs $\nu = 241.8$ THz circularly polarized laser pulse, all-optical, $T = 175$ K
Garnet [26]	–	$\tau^{\text{switching}}_{\text{field}} \lesssim 100$ fs	–	100 fs $\nu = 372.41$ THz linear and circularly-polarized laser pulse, $T = 300$ K, all-optical, MRev
GdFeCo [28]	–	$\tau^{\text{switching}}_{\text{field}} \sim$ subpicosecond	–	40 fs $\nu = 374.74$ THz circularly polarized laser pulse, $T = 300$ K, $T_C = 500$ K, all-optical, MRev
GdFeCo [39]	–	$\tau^{\text{switching}}_{\text{field}} = 700$ fs	–	500 fs $\nu = 374.74$ THz laser pulse, $T = 10 - 300$ K, athermal all-optical
GdFeCo [30]	–	$\tau^{\text{switching}}_{\text{field}} = 30$ ps	–	100 fs $\nu = 374.74$ THz circularly polarized laser pulse, $T = 10$ K, all-optical
GdFeCo [34]	–	–	–	100 fs $\nu = 374.74$ THz circularly polarized laser pulse, $T = 300 - T_C$ K, all-optical
Gd_2O_3 [40]	–	–	≈ 0.1 ns(*)	thermal, 5–10 nm nanoparticles, $T = 285-287$ K
Ni [41]	–	–	0.055ns(*)	thermal, 3.8 nm nanoparticles, $T = 310$ K
Fe [42]	–	–	(0.1±0.05)ns(*)	thermal and field, (2.9 ±0.3)nm nanoparticles, $T = 80$ K
Co [43]	–	–	0.1 ns(*)	thermal and field, (25±5) nm-diameter nanoparticles, $T = 0.1 - 6$ K

thermore, our Eq. (49) suggests that the field-driven switching rate, which would correspond also to a resonance frequency of the nutation mode, increases monotonically with temperature. A spin resonance mode with such temperature dependence has in fact been observed in Ref. [25] (referred to as a "quasi-AFM mode" represented by filled circles in Fig. 3 of Ref. [25]), but with a much lower frequency range (few hundreds of GHz) than that expected based on our theory (few hundreds of THz). This can be partly attributed to the magnetic domain size, which is in the μm scale in Ref. [25] rather than the Å scale assumed in our calculation, as larger volume gives rise to lower field-driven switching rate or resonance frequency, according to our Eq. (49).

The last part of Table III on the bottom pertains to the thermal switching time, commonly referred to as superparamagnetic relaxation time in the literature. The available data indicate a timescale mostly in the order of nanosecond. This is partly due to the fact that the systems under studies in Refs. [41,43] mostly involve magnetic particles with sizes in the nanometer regime, giving larger volume v than what we used in Table I. According to Eq. (48), to leading order, this will reduce the relaxation rate and thus increase the relaxation time, relative to our theoretical numbers presented in Table III, for which subnanometer size has been assumed. More precisely, according to Eq. (48), thermal switching time is proportional to the magnetic volume v. Since the experimental volume is in the nm^3 regime while our calculation assumes the Å^3 regime, we expect experimental thermal switching time to be at least $10^3 = 1000$ times larger than our values, in agreement with the data presented in Table III. Furthermore, comparing the available data on the four elemental ferromagnets, especially the three transition metal ferromagnets (omitting the ± 0.05 ns uncertainty in the result for Fe), the relaxation time for Ni is found to be the smallest between those of Fe, Ni, and Co, in precise agreement with our theoretical prediction. Data for Gd nanoparticles are not available; only data for compound Gd_2O_3 is listed, for which direct comparison with the theoretical result for Gd should not be made. It can be seen that, while the present paper is not aimed at reproducing every available experimental data quantitatively, our theory gives some penetrating insights and conceptual framework for understanding experimental observations and available data on ultrafast magnetism phenomena at elevated temperatures.

VIII. DISCUSSION AND CONCLUSIONS

We have developed an accurate model for describing magnetization dynamics in ferromagnetic materials under Curie temperature and in an ultrafast regime, where inertial effect must be taken into account. Our main results demonstrate that in the ultrafast regime, a new mode of magnetization reversal corresponding to nutation emerges persists against thermal fluctuations that reduce the stability of the former, requiring only ac field to generate it and gives rise to the fastest switching rate proportional to the ac field frequency. Stable reversal of magnetization state can be realized by the application of a *pulse* of ac field of finite duration $\Delta t = (2n+1)T_{\text{period}}/2$ where $n = 0, 1, 2, 3, \cdots$.

Our finding that a stationary alternating (ac) field induces magnetization reversal even in the absence of static field explains the experimental observation of magnetization reversal induced by laser pulse without any static field [28], by simple extension of our theory to $H_{\text{ac}}(x,t) \sim \cos(\omega t - kx)$. The subpicosecond timescale for magnetic switching found in our work naturally explains the femtosecond timescale of all-optical magnetic switching [25,29,34]. Furthermore, the observation that circularly polarized light is able to drive the reversal while the linearly polarized one is not follows naturally from the fact that at any direction in the yz plane normal to the wave propagation direction x, the circular polarization always projects a nonzero alternating optomagnetic field along the magnetization direction $\mathbf{m}$, taken to be along the z axis, for example, whereas a linearly polarized light has zero projection in direction z if the linear polarization direction is along y. In this illustration, linearly polarized light with polarization direction on yz plane away from y axis can still induce a magnetization reversal. Our exposition of the thermal-driven and field-driven modes also demonstrates that both temperature and field effects play roles in experiments [22,23]. In particular, lower critical $H_{0\text{ac}}$ required for the nutation switching mode at lower temperatures implies lower laser fluence as well, in agreement with experimental findings [29]. Our results provide a transparent macroscopic picture of ultrafast magnetization reversal dynamics relying on alternating field or optical waves and will motivate further works to realize ultra-high-speed magnetic devices.

ACKNOWLEDGMENTS

I.M. acknowledges funding from the French Agence Nationale de la Recherche (ANR) through project ANR-ICEMAN under Grant No. 19-CE05-0019-01 for his work at IM2NP Marseille. I.M. also thanks PROMES Perpignan for hospitality and financial support of his visit while thanking Professor H. Kachkachi, Professor F. Vernay, and Dr. R. Bastardis for very insightful discussions.

APPENDIX A: DERIVATION OF COMPONENTS OF CURRENT DENSITY VECTOR

Noting that $\mathbf{H}_{\text{eff}} = -\partial V/\partial \mathbf{m}$, the LLG part of the iLLGB equation

$$\gamma_0(\mathbf{m} \times (\mathbf{H}_{\text{eff}} + \mathbf{h}(t))) - \frac{\alpha_\perp}{m^2}[\mathbf{m} \times \dot{\mathbf{m}}] \tag{A1}$$

is equivalent to

$$\gamma_0 \mathbf{m} \times \left(-\frac{\partial V}{\partial \mathbf{m}} + \mathbf{h}(t)\right) - \frac{\alpha_\perp \gamma_0}{m^2}\mathbf{m} \times \left(\mathbf{m} \times \left(-\frac{\partial V}{\partial \mathbf{m}} + \mathbf{h}(t)\right)\right), \tag{A2}$$

where

$$m = |\mathbf{m}| = m_r. \tag{A3}$$

In the intuitive derivation of the Fokker-Planck equation [36], the effect of stochastic field $\mathbf{h}(t)$ is already represented by the thermal diffusion term $-k'\nabla\rho$. The terms

involving $\mathbf{h}(t)$ in Eqs. (7), (A1), and (A2) are thus not furthermore evaluated as their equivalent $-k'\nabla\rho$ will be added at the end of this Appendix. We evaluate the remaining term by term of Eq. (A2) in a spherical coordinate system, which produces the following equation:

$$-\mathbf{m}\times\frac{\partial V}{\partial \mathbf{m}}=\left(\frac{1}{\sin\theta}\frac{\partial V}{\partial\phi}\right)\hat{e}_\theta+\left(-\frac{\partial V}{\partial\theta}\right)\hat{e}_\phi, \tag{A4}$$

noting that $\mathbf{m}=m_r\hat{e}_r$. So,

$$\begin{aligned}\gamma_0(\mathbf{m}\times\mathbf{H}_{\rm eff})&=-\gamma_0\mathbf{m}\times\frac{\partial V}{\partial\mathbf{m}}\\&=\gamma_0\left[\left(\frac{1}{\sin\theta}\frac{\partial V}{\partial\phi}\right)\hat{e}_\theta+\left(-\frac{\partial V}{\partial\theta}\right)\hat{e}_\phi\right]\end{aligned} \tag{A5}$$

becomes, after transformation from Landau-Lifshitz-Gilbert back to Landau-Lifshitz form:

$$\gamma_0\left[\left(\frac{1}{\sin\theta}\frac{\partial V}{\partial\phi}\right)\hat{e}_\theta+\left(-\frac{\partial V}{\partial\theta}\right)\hat{e}_\phi\right]. \tag{A6}$$

The Bloch term in spherical coordinates is given by

$$+\frac{\gamma_0\alpha_\parallel}{m_r^2}(\mathbf{m}\cdot\mathbf{H}_{\rm eff})\mathbf{m}=-\frac{\gamma_0\alpha_\parallel}{m_r}m_r\hat{e}_r\frac{\partial V}{\partial m_r}. \tag{A7}$$

The Gilbert damping term in spherical coordinates upon transformation into Landau-Lifshitz form is given by

$$\begin{aligned}&-\frac{\alpha_\perp}{m^2}[\gamma_0\mathbf{m}\times(\mathbf{m}\times\mathbf{H}_{\rm eff})]\\&=-\frac{\alpha_\perp\gamma_0}{m_r}\left[\frac{1}{\sin\theta}\frac{\partial V}{\partial\phi}\hat{e}_\phi+\frac{\partial V}{\partial\theta}\hat{e}_\theta\right].\end{aligned} \tag{A8}$$

The inertial term becomes, after a rather tedious algebraic manipulation,

$$\begin{aligned}-\frac{\alpha_\perp}{m_r^2}[\tau\mathbf{m}\times\mathbf{m}]=&-\frac{\alpha_\perp\tau\gamma_0^2}{m_r}\frac{\partial V}{\partial m_r}\left(\frac{1}{\sin\theta}\frac{\partial V}{\partial\phi}\hat{e}_\theta-\frac{\partial V}{\partial\theta}\hat{e}_\phi\right)\\&+\alpha_\perp\gamma_0\tau\left(\frac{\partial^2 V}{\partial t\,\partial m_r}\mathbf{m}-\frac{\partial}{\partial t}\frac{\partial V}{\partial\mathbf{m}}\right),\end{aligned} \tag{A9}$$

with

$$\frac{\partial V}{\partial\mathbf{m}}=\frac{\partial V}{\partial m_r}\hat{e}_r+\frac{1}{m_r}\frac{\partial V}{\partial\theta}\hat{e}_\theta+\frac{1}{m_r\sin\theta}\frac{\partial V}{\partial\phi}\hat{e}_\phi, \tag{A10}$$

where we have applied zeroth order approximation for which we omit $\partial m_r/\partial t$ when evaluating $\mathbf{m}$. In this case, the inertial term contributes to the fully transverse spin torque (or velocity of the magnetic particle in the language of Brown theory):

$$\begin{aligned}-\frac{\alpha_\perp}{m_r^2}[\tau\mathbf{m}\times\mathbf{m}]\simeq&-\frac{\alpha_\perp\tau}{m_r}\left(-\frac{\gamma_0^2}{\sin\theta}\frac{\partial V}{\partial m_r}\frac{\partial V}{\partial\phi}+\gamma_0\frac{\partial^2 V}{\partial t\,\partial\theta}\right)\hat{e}_\theta\\&-\frac{\alpha_\perp\tau}{m_r}\left(\gamma_0^2\frac{\partial V}{\partial m_r}\frac{\partial V}{\partial\theta}+\frac{\gamma_0}{\sin\theta}\frac{\partial^2 V}{\partial t\,\partial\phi}\right)\hat{e}_\phi.\end{aligned} \tag{A11}$$

Eventually, we will consider time-dependent potential energy to accommodate time-dependent ac magnetic field or electromagnetic field to drive switching or the collective mode of interest. The expression Eq. (A11) was obtained by retaining only time dependence due to the ac field applied along a fixed direction along $\hat{z}$, whereas the time dependence due to dynamical fluctuation of m_r as well as time dependence of θ and ϕ are subleading to that of the ac field.

The above equations give the spherical coordinate components of the Brown particle current density vector in the absence of thermal agitations:

$$J_r=-\rho\gamma_0\alpha_\parallel\frac{\partial V}{\partial m_r}, \tag{A12}$$

$$J_\theta=\frac{\rho\gamma_0}{\sin\theta}\left(1+\frac{\alpha_\perp\tau\gamma_0}{m_r}\frac{\partial V}{\partial m_r}\right)\frac{\partial V}{\partial\phi}-\rho\frac{\alpha_\perp\gamma_0}{m_r}\left(1+\tau\frac{\partial}{\partial t}\right)\frac{\partial V}{\partial\theta}, \tag{A13}$$

$$J_\phi=-\rho\gamma_0\left(1+\frac{\alpha_\perp\tau\gamma_0}{m_r}\frac{\partial V}{\partial m_r}\right)\frac{\partial V}{\partial\theta}-\frac{\rho\alpha_\perp\gamma_0}{m_r\sin\theta}\left(1+\tau\frac{\partial}{\partial t}\right)\frac{\partial V}{\partial\phi}. \tag{A14}$$

The effective conservative potential is $V(m_r,\theta,\phi)$ in spherical coordinates.

APPENDIX B: DERIVATION OF ANALYTICAL SOLUTION OF FOKKER-PLANCK EQUATION WITH CONSTANT POTENTIAL

Considering a (hypothetical) constant potential $V(x,y,t)=V_0$, one can use the method of separation of variables to solve for the $\rho[x,y,t]$ by writing $\rho[x,y,t]=X(x)Y(y)T(t)$. We obtain the following set of ordinary differential equations:

$$(x^2-1)\frac{d^2X(x)}{dx^2}+2x\frac{dX(x)}{dx}-\text{const}_2X[x]=0, \tag{B1}$$

$$y^2\frac{d^2Y(y)}{dy^2}+2y\frac{dY(y)}{dy}-\left(\frac{\text{const}_1}{k'}y^2+\text{const}_2\right)Y[y]=0 \tag{B2}$$

$$\frac{dT(t)}{dt}-\text{const}_1T(t)=0, \tag{B3}$$

where const_1, const_2 are constants to be determined (eventually acting as the eigenvalues of the corresponding eigenvalue problem). In fact, Eq. (B1) takes exactly the form of the Legendre equation when $\text{const}_2=n(n+1)$ while Eq. (B2) takes exactly the form of the spherical Bessel function when $\text{const}_1=-k'$, $\text{const}_2=n(n+1)$. In fact, any $\text{const}_1=-sk'$ with scaling factor s still gives a spherical Bessel function with appropriate rescaling of y. It will be seen later when considering expanding the full solution for $\rho(x,y,t)$ that we have to choose $s=u^2_{-n-1,\alpha}$, where $u^2_{-n-1,\alpha}$is the αth zero of spherical Bessel function $\mathcal{Y}_{-n-1}(y)$.

The solutions of the above set of ordinary differential equations are

$$T(t)=C_te^{\text{const}_1t}, \tag{B4}$$

$$\begin{aligned}X[x]=&C_{xP}P\left[\frac{(-1+\sqrt{1+4\text{const}_2})}{2},x\right]\\&+C_{xQ}\mathrm{Q}\left[\frac{(-1+\sqrt{1+4\text{const}_2})}{2},x\right],\end{aligned} \tag{B5}$$

$$Y[y] = C_{yJ}\mathcal{J}\left[\frac{(-1-\sqrt{1+4\text{const}_2})}{2}, -\frac{i\sqrt{\text{const}_1}y}{\sqrt{k'}}\right] + C_{yY}\mathcal{Y}\left[\frac{(-1-\sqrt{1+4\text{const}_2})}{2}, -\frac{i\sqrt{\text{const}_1}y}{\sqrt{k'}}\right], \tag{B6}$$

where $C_t, C_{xP}, C_{xQ}, C_{yJ}, C_{yY}$ are constants to be determined by boundary and initial conditions as well as physical constraints such as analytic behavior to give a nondivergent result, $P[\lambda, x]$, $Q[\lambda, x]$ represent the Legendre polynomial and Legendre function of the second kind, respectively. Both functions impose that the degree λ be integer $\lambda = n = 0, 1, 2, 3, \cdots$, giving a quantized value for $\text{const}_2 = n(n+1)$. They are, respectively, given by

$$P[n, x] = P_n(x) = \frac{1}{2^n n!}\frac{d^n}{dx^n}(x^2-1)^n = \frac{1}{2^n}\sum_{k=0}^{n}\left(\frac{n!}{k!(n-k)!}\right)^2 (x-1)^{n-k}(x+1)^k, \tag{B7}$$

$$Q_0(x) = \frac{1}{2}\ln\frac{1+x}{1-x}, \tag{B8}$$

$$Q_1(x) = P_1(x)Q_0(x) - 1, \tag{B9}$$

$$Q_n = \frac{2n-1}{n}xQ_{n-1}(x) - \frac{n-1}{n}Q_{n-2}(x), \quad n \geqslant 2, \tag{B10}$$

which suggests that the full solution for the x-dependent function $X(x) \equiv X(\theta)$ involves both polynomial and logarithmic functions of $x = \cos\theta$. Both functions are singular at $x = \pm 1$, corresponding to $\theta = 0, \pi$, precisely where the minima of the actual potential $V(\theta)$ we have in our problem are located.

On the other hand, $\mathcal{J}, \mathcal{Y}$ represent spherical Bessel functions, solutions of the differential equation

$$y^2\frac{d^2Y(y)}{dy^2} + 2y\frac{dY(y)}{dy} + (y^2 - n(n+1))Y[y] = 0, \tag{B11}$$

with solutions

$$\mathcal{J}[n, y] = j_n(y) = \sqrt{\frac{\pi}{2y}}J_{n+\frac{1}{2}}(y), \tag{B12}$$

$$\mathcal{Y}[n, y] = y_n(y) = \sqrt{\frac{\pi}{2y}}Y_{n+\frac{1}{2}}(y) = (-1)^{n+1}\sqrt{\frac{\pi}{2y}}J_{-n-\frac{1}{2}}(y), \tag{B13}$$

in terms of the ordinary Bessel functions J_n and Y_n.

The occurrence of the Legendre polynomial for the solution of the $x = \cos\theta$ part is well expected due to the axial symmetry of the system. Since the Legendre polynomial is quantized in discrete integers, this imposes a constraint on the value of const_2. On the other hand, the const_1 acts as the eigenvalue of the temporal part of the set of differential equations. The full solution of the partial differential equation Eq. (33) for constant potential V is

$$\rho[x, y, t] = X_0(x)Y_0(y)T_0(t) + \sum_{n=1}^{\infty}X_n(x)Y_n(y)T_n(t). \tag{B14}$$

The basis functions are given by Eqs. (B5) and (B6) for the x and y parts, respectively, which give, imposing the physical condition of finite magnetic particle density everywhere in the interval $x \in [-1, 1]$, $y \in [0, 1]$ gives rise to

$$u_n^x(x) = c_{Pn}P_n(x), \tag{B15}$$

$$u_{n\alpha}^y(y) = c_{Yn\alpha}\mathcal{Y}_{-n-1}(u_{-n-1,\alpha}y), \tag{B16}$$

taking into account the fact that the Legendre Q and spherical Bessel J functions both are singular in the respective intervals. The overall coefficients c_{Pn}, c_{Yn} are fixed by imposing the normalization condition,

$$\int_{-1}^{1}dx u_n^x(x)u_m^x(x) = \delta_{nm}, \tag{B17}$$

$$\int_0^1 dy y^2 u_{n\alpha}^y(y)u_{n\beta}^y(y) = \delta_{\alpha\beta}, \tag{B18}$$

where the presence of y^2 in the last equation is to be noted, reflecting the fact that the spherical Bessel function pertains to spherical coordinates. Furthermore, spherical Bessel functions of the same index n are orthogonal to each other if their zeros are different ($\alpha \neq \beta$).

Using standard identity [54],

$$\int_0^1 dx P_n(x)P_m(x) = \frac{2}{2n+1}\delta_{nm}, \tag{B19}$$

we obtain

$$c_{Pn} = \sqrt{\frac{2n+1}{2}}. \tag{B20}$$

On the other hand, for the y part, we employ the orthogonality relation for spherical Bessel function

$$\int_0^1 dy y^2 \mathcal{Y}_n(u_{n,\alpha}y)\mathcal{Y}_n(u_{n,\beta}y) = \frac{1}{2}\delta_{\alpha\beta}[\mathcal{Y}_{n+1}(u_{n,\alpha})]^2, \tag{B21}$$

where $u_{n,\alpha}$ represents the αth zero of $\mathcal{Y}[n, y]$. Substituting Eqs. (B16) and (B21) into Eq. (B18), we obtain

$$c_{Yn\alpha} = \frac{\sqrt{2}}{\mathcal{Y}_{-n}(u_{-n-1,\alpha})} \tag{B22}$$

for $n = 1, 2, 3, \cdots$. The y part of the solution involves the spherical Bessel function. Expansion in terms of Bessel functions of a given n but different zeros α (forming the Bessel series) follows from the orthogonality relation for such spherical Bessel functions. In this paper, we will extensively use the asymptotic form of Bessel function

$$J_\nu(z) \simeq \sqrt{\frac{2}{\pi z}}\cos\left(z - \frac{\nu\pi}{2} - \frac{\pi}{4}\right) \tag{B23}$$

for $z \gg |n^2 - 1/4|$, which has zeros at

$$u_{-n-1,\alpha} = \left(\frac{n}{2} + \alpha + 1\right)\pi, \tag{B24}$$

and $\alpha = 0, 1, 2, 3, \ldots$. Substituting Eqs. (B23)–(B24) into Eq. (B22) gives

$$c_{Yn\alpha} = (-1)^{n-\alpha-2}\sqrt{2}\left(\frac{n}{2}+\alpha+1\right)\pi. \tag{B25}$$

The full solution Eq. (B14) now explicitly takes the form

$$\rho(x,y,t) = \rho_0(x,y) + \sum_{n=1}^{\infty}\sum_{\alpha=0}^{\infty} c_{n\alpha}\mathcal{Y}_{-n-1}(u_{-n-1,\alpha}y)P_n(x)e^{-p_n t}, \tag{B26}$$

where $x = \cos\theta$, $y = m_r$, and $c_{n\alpha}$ depends on the initial condition $\rho(x, y, t = 0)$ at $t = 0$. The coefficient is given by

$$c_{n\alpha} = \frac{2n+1}{[\mathcal{Y}_{-n}(u_{-n-1,\alpha})]^2}\int_0^1 dy y^2 \int_{-1}^1 dx \delta\rho(x,y,t=0)P_n(x), \times \mathcal{Y}_{-n-1}(u_{-n-1,\alpha}y) \tag{B27}$$

where $u_{-n-1,\alpha}$ is the αth zero of the spherical Bessel function $\mathcal{Y}_{-m-1}(y)$. Alternatively, we may expand the solution in terms of the J Bessel function

$$\delta\rho(x,y,t) = \sum_{n=0}^{\infty}\sum_{\alpha=0}^{\infty}\tilde{c}_{n\alpha}J_{n+\frac{1}{2}}\left(u_{n+\frac{1}{2},\alpha}y\right)P_n(x)e^{-p_n t}, \tag{B28}$$

with the coefficient

$$\tilde{c}_{n\alpha} = \frac{2n+1}{\left[J_{n+\frac{3}{2}}(u_{n+\frac{1}{2},\alpha})\right]^2}\int_0^1 dy y\int_{-1}^1 dx\delta\rho(x,y,t=0) \times J_{n+\frac{1}{2}}(u_{n+\frac{1}{2}\alpha}y)P_n(x), \tag{B29}$$

where $u_{n+\frac{1}{2},\alpha}$ is the αth zero of $J_{n+\frac{1}{2}}(y)$. The J and spherical $\mathcal{Y}$ Bessel functions are related by

$$\mathcal{Y}_{\tilde{n}}(x) = (-1)^{\tilde{n}+1}\sqrt{\frac{\pi}{2y}}J_{-\tilde{n}-\frac{1}{2}}(y), \tag{B30}$$

in which $\tilde{n} = -n-1$.

APPENDIX C: CALCULATIONS FOR PERTURBATIVE SOLUTION OF FOKKER-PLANCK EQUATION WITH THE ACTUAL POTENTIAL

This Appendix gives the details of the perturbative analytical solution to the Fokker-Planck equation with the actual magnetic potential energy. Readers not interested in these mathematical details can skip this Appendix altogether.

Turning on the static field, alternating field, longitudinal relaxation, and anisotropy terms, we obtain additional terms entering the partial differential equation

$$\begin{aligned}
&\frac{\alpha_\perp\gamma_0}{k'M_s}\left(M_s(H_0+H_{\rm ac}(t))+\frac{M_s^2}{\chi_\perp}xy\right)(1-x^2)y\frac{\frac{dX_n(x)}{dx}}{X_n(x)}\\
&+\frac{\alpha_\perp\tau\gamma_0}{k'}(1-x^2)y\frac{dH_{\rm ac}(t)}{dt}\frac{1}{X_n(x)}\frac{dX_n(x)}{dx}\\
&-\frac{\alpha_\perp\gamma_0}{k'M_s}\left(2xyM_s(H_0+H_{\rm ac}(t))+2M_s\tau xy\frac{\partial H_{\rm ac}(t)}{\partial t}\right)\\
&-\frac{\alpha_\perp\gamma_0}{k'M_s}\left(\frac{2M_s^2}{\chi_\perp}x^2y^2-\frac{M_s^2}{\chi_\perp}(1-x^2)y^2\right)
\end{aligned} \tag{C1}$$

for the x part of the full partial differential equation and

$$\begin{aligned}
&-\frac{\alpha_\parallel\gamma_0}{k'M_s}\left(M_s(H_0+H_{\rm ac}(t))+\frac{M_s^2}{\chi_\perp}xy\right)xy^2\frac{1}{Y_n(y)}\frac{dY_n(y)}{dy}\\
&+\left(\frac{\alpha_\parallel M_s\gamma_0}{2\chi_\parallel k'}(y^2-y_e^2)y^3+\frac{\alpha_\parallel M_s\gamma_0}{\chi_\perp k'}(1-x^2)y^3\right)\frac{\frac{dY_n(y)}{dy}}{Y_n(y)}\\
&-2\frac{\alpha_\parallel\gamma_0}{k'}(H_0+H_{\rm ac}(t))xy+3\frac{\alpha_\parallel M_s\gamma_0}{k'\chi_\perp}y^2(1-x^2)\\
&+\frac{\alpha_\parallel M_s\gamma_0}{2k'\chi_\parallel}\left(3y^2(y^2-y_e^2)+2y^4\right)
\end{aligned} \tag{C2}$$

for the y part of the full partial differential equation, which makes the full partial differential equation not exactly analytically solvable in general. In fact, is is found that any finite nonzero value of $H_0, H_{\rm ac}, 1/\chi_\perp, 1/\chi_\parallel$ would preclude the exact analytical solution of the partial differential equation. We thus resort to the perturbative solution described in the following section.

We adopt the perturbative method outlined in Ref. [39] but in a generalized form where the perturbation term appears not only as a term multiplying the (perturbed) eigenfunction but also involves a (perturbative) differential operator acting on the perturbed eigenfunction. More precisely, the full Fokker-Planck Eq. (33) can be written as an eigenvalue problem,

$$\begin{aligned}
&L_x(\overline{u}_n^x(x)) + \delta L_x(\overline{u}_n^x(x)) - \epsilon_x r_x(x,y)(\overline{u}_n^x(x)) + \overline{\lambda}_n^x(\overline{u}_n^x(x))\\
&+L_y(\overline{u}_n^y(y))+\delta L_y(\overline{u}_n^y(y))-\epsilon_y r_y(x,y)(\overline{u}_n^y(y))\\
&+\overline{\lambda}_n^y(\overline{u}_n^y(y)) = 0,
\end{aligned} \tag{C3}$$

while the unperturbed Fokker-Planck equations in terms of x and y parts are given by Eqs. (B1) and (B2) that, respectively, can be written as

$$L_x(u_n^x(x)) + \lambda_n^x u_n^x(x) = 0, \tag{C4}$$

$$L_y(u_{n\alpha}^y(y)) + \lambda_n^y u_{n\alpha}^y(y) = 0 \tag{C5}$$

for any αth zero of the spherical Bessel function which gives the y part of the eigenfunction $u_{n\alpha}^y(y)$. In the equations above, $u_n^x(x)(\overline{u}_n^x(x))$, respectively, represent the unperturbed (perturbed) eigenfunctions (for the x part, similarly for the y part), $L_x(\overline{u}_n^x(x))$, $\delta L_x(\overline{u}_n^x(x))$ represent, respectively the unperturbed (and perturbative) differential operators acting on the (perturbed) eigenfunctions (for the x part, similarly for the y part), $\epsilon_{x(y)}$ the perturbation small parameter for $x(y)$ part, $r_{x(y)}(x,y)$ the perturbative function (not differential operator) multiplying the (perturbed) eigenfunction, while $\overline{\lambda}_n^{x(y)}$, $\lambda_n^{x(y)}$ the perturbed (unperturbed) eigenvalues of the corresponding eigenvalue problems. The eigenvalues are given by

$$\lambda_n^x = -n(n+1), \quad \lambda_{n\alpha}^y = -\frac{n(n+1)}{u_{-n-1,\alpha}^2}, \tag{C6}$$

where the latter can be shown via a little algebraic exercise starting from the differential equation defining the spherical Bessel function,

$$y^2\frac{d^2Y(y)}{dy^2}+2y\frac{dY(y)}{dy}+(y^2-n(n+1))Y(y) = 0, \tag{C7}$$

where $\lambda_n = -n(n+1)$ acts as the eigenvalue. We then scale the variable as follows: $y \to u_{n,\alpha} y$. It is easy to show that $Y(u_{n,a}y)$ also satisfies the above equation but with eigenvalue $\lambda_{n\alpha} = -n(n+1)/u^2_{n,\alpha}$.

The unperturbed eigenfunctions are given by Eqs. (B15) and (B16) for the x and y parts respectively. The perturbation differential operators and multiplying functions are obtained from Eqs. (C1) and (C2) and are given by

$$\begin{aligned}
&\delta L_x\big(\overline{u}^x_n(x)\big) \\
&\quad = \frac{\alpha_\perp \gamma_0}{k' M_s}\left(M_s(H_0 + H_{\rm ac}(t)) + \frac{M_s^2}{\chi_\perp} xy\right)(1-x^2) y \frac{d\overline{u}^x_n(x)}{dx} \\
&\qquad + \frac{\alpha_\perp \tau \gamma_0}{k'}(1-x^2) y \frac{dH_{\rm ac}(t)}{dt}\frac{d\overline{u}^x_n(x)}{dx}, \qquad \text{(C8)} \\
&\delta L_y\big(\overline{u}^y_n(y)\big) \\
&\quad = -\frac{\alpha_\parallel \gamma_0}{k' M_s}\left(M_s(H_0 + H_{\rm ac}(t)) + \frac{M_s^2}{\chi_\perp} xy\right) xy^2 \frac{d\overline{u}^y_n(y)}{dy} \\
&\qquad + \frac{\alpha_\parallel M_s \gamma_0}{2k' \chi_\parallel}\big(3y^2\big(y^2 - y_e^2\big) + 2y^4\big)\frac{d\overline{u}^y_n(y)}{dy} \qquad \text{(C9)} \\
&-\epsilon_x r_x(x,y) \\
&\quad = -\frac{\alpha_\perp \gamma_0}{k' M_s}\left(2xy M_s(H_0 + H_{\rm ac}(t)) + 2M_s \tau xy \frac{\partial H_{\rm ac}(t)}{\partial t}\right) \\
&\qquad - \frac{\alpha_\perp \gamma_0}{k' M_s}\left(\frac{2M_s^2}{\chi_\perp} x^2 y^2 - \frac{M_s^2}{\chi_\perp}(1-x^2) y^2\right) \qquad \text{(C10)} \\
&-\epsilon_y r_y(x,y) \\
&\quad = -2\frac{\alpha_\parallel \gamma_0}{k'}(H_0 + H_{\rm ac}(t)) xy + 3\frac{\alpha_\parallel M_s \gamma_0}{k' \chi_\perp} y^2(1-x^2) \\
&\qquad + \frac{\alpha_\parallel M_s \gamma_0}{2k' \chi_\parallel}\big(3y^2\big(y^2 - y_e^2\big) + 2y^4\big). \qquad \text{(C11)}
\end{aligned}$$

Writing the resulting partial differential equation in the form of an eigenvalue problem, we will obtain an equation containing terms of different orders in ϵ_x, ϵ_y. Grouping them term by term, the zeroth order terms $O(\epsilon_x^0, \epsilon_y^0)$ are given by

$$\delta L_x\big(u^x_n(x)\big) + \delta L_y\big(u^y_{n\alpha}(y)\big) = 0. \qquad \text{(C12)}$$

The first-order terms $O(\epsilon_x, \epsilon_y)$ are given by

$$\begin{aligned}
&\epsilon_x\big[L_x\big(v^x_n(x)\big) + \delta L_x\big(v^x_n(x)\big) + \lambda^x_n v^x_n(x) - r_x(x,y) u^x_n(x)\big] \\
&\quad + \epsilon_x \mu^x_n(y) u^x_n(x) + \epsilon_y\big[L_y\big(v^y_{n\alpha}(y)\big)\big) \\
&\quad + \delta L_y\big(v^y_{n\alpha}(y)\big) + \lambda^y_n v^y_{n\alpha}(y)\big] \\
&\quad \times \epsilon_y\big[-r_y(x,y) u^y_{n\alpha}(y) + \mu^y_{n\alpha}(x) u^y_{n\alpha}(y)\big] = 0. \qquad \text{(C13)}
\end{aligned}$$

We will treat ϵ_x as independent of ϵ_y. As such, each line of Eq. (C13) must vanish, giving a form mimicking the standard first-order term in the perturbation theory for the eigenvalue problem with a single variable [39],

$$\begin{aligned}
&[L_x + \delta L_x] v^x_n(x) + \lambda^x_n v^x_n(x) \\
&\quad + \big[-r_x(x,y) + \mu^x_n(y)\big] u^x_n(x) = 0, \qquad \text{(C14)} \\
&[L_y + \delta L_y] v^y_{n\alpha}(y) + \lambda^y_{n\alpha} v^y_{n\alpha}(y) \\
&\quad + \big[-r_y(x,y) + \mu^y_{n\alpha}(x)\big] u^y_{n\alpha}(y) = 0, \qquad \text{(C15)}
\end{aligned}$$

where there are new terms corresponding to the perturbation differential operator terms $\delta L_x(v^x_n(x)), \delta L_y(v^y_n(y))$. Multiplying from the left Eq. (C14) with $u^x_l(x)$ and Eq. (C15) with $u^y_l(y)$ and integrating both over corresponding fundamental domain $\int dg = \int_{-1}^1 dx$ for Eq. (C14) and $\int dg = \int_0^1 dy y^2$ for Eq. (C15), we obtain for the expansion coefficient $a^x_{nl}(y)$ of the first-order correction to the eigenfunction,

$$v^x_n(x,y,t) = {\sum_l}' a^x_{nl}(y,t) u^x_l(x) \qquad \text{(C16)}$$

(where ${\sum_l}'$ means $l = n$ is excluded [39]) or

$$a^x_{nl}(y,t) = \int dg v^x_n(x,y,t) u^x_l(x), \qquad \text{(C17)}$$

the following expression:

$$a^x_{nl}(y,t) = \frac{1}{\lambda^x_n - \lambda^x_l}\big[d^x_{nl}(y,t) - \mu^x_n(y,t)\delta_{nl} - e^x_{nl}(y,t)\big], \qquad \text{(C18)}$$

where the y dependence in $a^x_{nl}(y)$ comes from that of

$$\begin{aligned}
d^x_{nl}(y) &= \int_{-1}^1 dx r_x(x,y) u^x_n(x) u^x_l(x), \qquad \text{(C19)} \\
e^x_{nl}(y) &= \int_{-1}^1 dx u^x_l(x) \delta L_x\big(v^x_n(x,y)\big), \qquad \text{(C20)} \\
\mu^x_n(y) &= d^x_{nn}(y) - e^x_{nn}(y). \qquad \text{(C21)}
\end{aligned}$$

Looking at Eq. (C18), the coefficient $a^x_{nl}(y,t)$ can be interpreted as the amplitude of the contribution of the eigenmode l to the perturbation of the eigenfunction of the eigenmode n due to the fields and thermal agitations. Since $\lambda_n = -n(n+1)$, the contribution decreases with l, more precisely with l^2 for large enough l, if we consider $n = 0, 1$ as the leading modes of interest.

The corresponding expressions for the y part are rather tricky, due to the fact that spherical Bessel functions are in general not orthogonal between each other. Only those spherical Bessel functions having the same index n but different orders (α, β) of its zeros are orthogonal to each other. As a result, the first-order correction of the eigenfunction for the y part is expanded as follows:

$$v^y_{n\alpha}(x,y,t) = {\sum_{l\beta}}' a^y_{nl;\alpha\beta}(x,t)\delta_{nl} u^y_{l\beta}(y) \qquad \text{(C22)}$$

(where ${\sum_{l\beta}}'$ means $\beta = \alpha$ is excluded [39]) or

$$a^y_{nl;\alpha\beta}(x,t) = \int dg v^y_{n\alpha}(x,y,t) u^y_{l\beta}(y); \qquad \text{(C23)}$$

the following expression:

$$a^y_{nl;\alpha\beta}(x)\delta_{nl}\left(\lambda^y_{n\alpha}-\lambda^y_{l\beta}\right) = d^y_{nl;\alpha\beta}(x)-\mu^y_{n\alpha}(x)(\delta_{nl}\delta_{\alpha\beta}+h_{nl;\alpha\beta}(1-\delta_{nl}))-e^y_{nl;\alpha\beta}(x), \tag{C24}$$

where the various factors appearing on the right-hand side are given by

$$d^y_{nl;\alpha\beta}(x)=\int_0^1 dy y^2 r_y(x,y)u^y_{n\alpha}(y)u^y_{l\beta}(y), \tag{C25}$$

$$e^y_{nl;\alpha\beta}(x,t)=\int_0^1 dy y^2 u^y_{l\beta}(y)\delta L_y(v^y_{n\alpha}(x,y)), \tag{C26}$$

$$h_{nl;\alpha\beta}=\int_0^1 dy y^2 u^y_{n\alpha}(y)u^y_{l\beta}(y). \tag{C27}$$

In this situation, we have three possible cases: (i) $n=l,\alpha=\beta$, (ii) $n=l,\alpha\neq\beta$, and (iii) $n\neq l$ regardless of α,β. Case (i) gives the expression for the first-order correction $\mu^y_{n\alpha}(x)$ to eigenvalue $\lambda^y_{n\alpha}$

$$\mu^y_{n\alpha}(x)=d^y_{nn;\alpha\alpha}(x)-e^y_{nn;\alpha\alpha}(x). \tag{C28}$$

Case (ii) gives the expression for the diagonal element $a_{nn;\alpha\beta}$ of the coefficient of expansion in Eq. (C22),

$$a^y_{nn;\alpha\beta}(x,t)=\frac{1}{\lambda^y_{n\alpha}-\lambda^y_{n\beta}}\left(d^y_{nn;\alpha\beta}(x)-e^y_{nn;\alpha\beta}\right), \tag{C29}$$

while the last case (iii) gives rise to the off-diagonal element of the coefficient of expansion in Eq. (C22),

$$a^y_{nl;\alpha\beta}=\frac{1}{\lambda^y_{n\alpha}-\lambda^y_{l\beta}}\left(d^y_{nl;\alpha\beta}(x)-\mu^y_{n\alpha}(x)h_{nl;\alpha\beta}-e^y_{nl;\alpha\beta}\right), \tag{C30}$$

which completes all coefficients of the expansion.

The expression for $a^x_{nl}(y)$ in Eq. (C18) cannot be evaluated explicitly because $v^x_n(x)$ is not yet known. In fact, one has to solve Eqs. (C16) and (C18) self-consistently. We will not pursue this self-consistent exact solution. Instead, we will employ an approximate solution by replacing $v^x_n(x)$ in Eq. (C18) with that obtained by setting δL_x to zero, as given in [39]

$$v^{(0)x}_n(x,y)=\sum_{j=1,j\neq n}^{\infty}\frac{d^x_{nj}(y)}{\lambda^x_n-\lambda^x_j}u^x_j(x) \tag{C31}$$

to be substituted into Eq. (C20). The corresponding expression for the y part is

$$v^{(0)y}_{n\alpha}(x,y)=\sum_{\beta=1,\beta\neq\alpha}^{\infty}\frac{d^y_{nn;\alpha\beta}(x)}{\lambda^y_{n\alpha}-\lambda^y_{n\beta}}u^y_{n\beta}(y). \tag{C32}$$

In both Eqs. (C31) and (C32), additional dependence shows up for the contribution from the ac field, giving $v^{(0)x}_n(x,y,t)$, $v^{(0)y}_{n\alpha}(x,y,t)$ due to $d^x_{nj}(y,t)$, $d^y_{nn;\alpha\beta}(x,t)$, respectively. This completes our perturbative solution calculation for our Fokker-Planck equation to first order in $\epsilon_{x(y)}\sim vM_sH_{0/0ac}/(k_BT)$, $vM_s^2/(\chi_{\perp/\parallel}k_BT)\ll 1$.

We evaluate the coefficients $a^{x(y)}_{nl}(y(x))$ and eigenvalue correction $\mu^{x(y)}_n(y(x))$ by first evaluating the coefficients $d^{x(y)}_{nl}(y(x))$, $\mu^{x(y)}_n(y(x))$, and $e^{x(y)}_{nl}(y(x))$ using the relevant equations given earlier. To this end, we first note that the perturbation multiplying function for x from Eq. (C10) can be rewritten as

$$-\epsilon_x r_x(x,y)=-\epsilon_x^{H_0}r_x^{H_0}(x,y)-\epsilon_x^{\chi_\perp}r_x^{\chi_\perp}(x,y)-\epsilon_x^{H_{ac}}r_x^{H_{ac}}(x,y), \tag{C33}$$

where

$$\epsilon_x^{H_0}=\frac{vM_sH_0}{k_BT}, \tag{C34}$$

$$r_x^{H_0}(x,y)=2\alpha_\perp\gamma_0\frac{k_BT}{k'vM_s}xy, \tag{C35}$$

$$\epsilon_x^{\chi_\perp}=\frac{vM_s^2}{\chi_\perp k_BT}, \tag{C36}$$

$$r_x^{\chi_\perp}(x,y)=\alpha_\perp\gamma_0\frac{k_BT}{k'vM_s}(3x^2-1)y^2, \tag{C37}$$

$$\epsilon_x^{H_{ac}}=\frac{vM_sH_{0ac}}{k_BT}, \tag{C38}$$

$$r_x^{H_{ac}}(x,y)=2\alpha_\perp\gamma_0\frac{k_BT}{k'vM_s}xy(\cos\omega t-\omega\tau\sin\omega t), \tag{C39}$$

which implies the fixed frequency ω of the ac field while varying its amplitude H_{0ac}. That is, we control the small parameter for the ac field only in terms of its amplitude.

On the other hand, the perturbative multiplying function for the y part can be rewritten as

$$-\epsilon_y r_y(x,y)=-\epsilon_y^{\chi_\perp}r_y^{\chi_\perp}(x,y)-\epsilon_y^{\chi_\parallel}r_y^{\chi_\parallel}(x,y)-\epsilon_y^{H}r_y^{H}(x,y), \tag{C40}$$

giving

$$\epsilon_y^{\chi_\perp}=\frac{vM_s^2}{\chi_\perp k_BT}, \tag{C41}$$

$$r_y^{\chi_\perp}(x,y)=-3\alpha_\parallel\gamma_0\frac{k_BT}{k'vM_s}(1-x^2)y^2, \tag{C42}$$

$$\epsilon_y^{\chi_\parallel}=\frac{vM_s^2}{\chi_\parallel k_BT}, \tag{C43}$$

$$r_y^{\chi_\parallel}(x,y)=-\frac{\alpha_\parallel\gamma_0}{2}\frac{k_BT}{k'vM_s}\left[3\left(y^2-y_e^2\right)+2y^2\right]y^2, \tag{C44}$$

$$\epsilon_y^{H_0}=\frac{vM_sH_0}{k_BT}, \tag{C45}$$

$$r_y^{H_0}(x,y)=2\alpha_\parallel\gamma_0\frac{k_BT}{k'vM_s}xy, \tag{C46}$$

$$\epsilon_y^{H_{ac}}=\frac{vM_sH_{0ac}}{k_BT}, \tag{C47}$$

$$r_y^{H_{ac}}(x,y)=2\alpha_\parallel\gamma_0\frac{k_BT}{k'vM_s}xy\cos\omega t. \tag{C48}$$

Substituting the above expressions for $r^{H_0,\chi_\perp,H_{0ac}}(x,y)$ into Eq. (C19) and using Eqs. (B15) and (B16), gives the following

expressions for $d_{nl}^{(H_0,\chi_\perp,H_{0ac})x}(y)$:

$$d_{nl}^{H_0,x}(y) = 2\alpha_\perp\gamma_0\frac{k_BT}{k'vM_s}c_{Pn}c_{Pl}y\int_{-1}^{1}dx x P_n(x)P_l(x) = 2\alpha_\perp\gamma_0\frac{k_BT}{k'vM_s}c_{Pn}c_{Pl}y\frac{n+l+1}{(2n+1)(2l+1)}(1-\delta_{nl})\delta_{n,l\pm1}, \tag{C49}$$

$$\begin{aligned} d_{nl}^{\chi_\perp,x}(y) &= \alpha_\perp\gamma_0\frac{k_BT}{k'vM_s}c_{Pn}c_{Pl}y^2\int_{-1}^{1}dx(3x^2-1)P_n(x)P_l(x) \\ &= 3\alpha_\perp\gamma_0\frac{k_BT}{k'vM_s}c_{Pn}c_{Pl}y^2\frac{\frac{2(n+1)(n+2)}{2n+3}\delta_{n,l-2}+\frac{2(n-1)n}{2n-1}\delta_{l,n-2}}{(2n+1)(2l+1)} + \alpha_\perp\gamma_0\frac{k_BT}{k'vM_s}c_{Pn}c_{Pl}y^2\left(\frac{3\left(\frac{2(n+1)^2}{(2n+3)}+\frac{2n^2}{2n-1}\right)}{(2n+1)(2l+1)}-\frac{2}{2n+1}\right)\delta_{nl}, \end{aligned} \tag{C50}$$

$$\begin{aligned} d_{nl}^{H_{0ac},x}(y,t) &= 2\alpha_\perp\gamma_0\frac{k_BT}{k'vM_s}c_{Pn}c_{Pl}y(\cos\omega t-\omega\tau\sin\omega t)\int_{-1}^{1}dx x P_n(x)P_l(x) \\ &= 2\alpha_\perp\gamma_0\frac{k_BT}{k'vM_s}c_{Pn}c_{Pl}y(\cos\omega t-\omega\tau\sin\omega t)\frac{n+l+1}{(2n+1)(2l+1)}(1-\delta_{nl})\delta_{n,l\pm1}, \end{aligned} \tag{C51}$$

while substituting Eqs. (C40)–(C48) into the corresponding expression for $d_{nl;\alpha\beta}^{\chi_\perp y}(x)$, $d_{nl;\alpha\beta}^{\chi_\parallel y}(x)$, one obtains

$$d_{nl;\alpha\beta}^{\chi_\perp,y}(x) = -3\alpha_\parallel\gamma_0\frac{k_BT}{k'vM_s}(x^2-1)c_{Yn\alpha}c_{Yl\beta}I_{nl;\alpha\beta}^{\chi_\perp}, \tag{C52}$$

where

$$\begin{aligned} I_{nl;\alpha\beta}^{\chi_\perp} &= \int_0^1 dy y^4\mathcal{Y}_{-n-1}(u_{-n-1,\alpha}y)\mathcal{Y}_{-l-1}(u_{-l-1,\beta}y) \\ &\simeq \frac{(-1)^{-(n+l)}}{u_{-n-1,\alpha}u_{-l-1,\beta}}\int_0^1 dy y^2\cos\left(u_{-n-1,\alpha}y-(n+1)\frac{\pi}{2}\right)\cos\left(u_{-l-1,\beta}y-(l+1)\frac{\pi}{2}\right), \end{aligned} \tag{C53}$$

where to get a simple closed-form analytical expression exactly, for general n, l, we have evaluated this expression approximately using the standard relation Eq. (B30) between the spherical $\mathcal{Y}$ and regular J Bessel functions of the first kind. The final result is

$$\begin{aligned} I_{nl;\alpha\beta}^{\chi_\perp} \simeq{}& \frac{(-1)^{l+n}\frac{4}{\pi^2}}{w_{ln,\beta\alpha}}\left(\frac{(-1)^{\alpha+\beta}}{(2\alpha-2\beta-l+n)^2}-\frac{(-1)^{\alpha+\beta}}{(4+2\alpha+2\beta+l+n)^2}\right) \\ &+\frac{(-1)^{l+n}\frac{4}{\pi^3}}{w_{ln,\beta\alpha}}\left(\frac{2\sin[(l-n)\frac{\pi}{2}]}{(2\alpha-2\beta-l+n)^3}+\frac{2\sin[(l+n)\frac{\pi}{2}]}{(4+2\alpha+2\beta+l+n)^3}\right), \end{aligned} \tag{C54}$$

where $w_{ln,\beta\alpha} = u_{-l-1,\beta}u_{-n-1,\alpha}$ and

$$u_{-n-1,\alpha} = \left(\frac{n}{2}+\alpha+1\right)\pi, \tag{C55}$$

with $\alpha = 0, 1, 2, 3, \cdots$ and likewise for $u_{-l-1,\beta}$ have been used. All the final expressions for perturbation coefficients in this calculation carry the indices n, l (and also α, β for the y part) and depend explicitly on them. The analytical expressions of those coefficients may at first glance contain terms that are singular for certain values of $n, l; \alpha, \beta$, such as $I_{nl;\alpha\beta}^{\chi_\perp}$ in Eq. (C54) which contains terms which become singular when $n = l, \alpha = \beta$. Such terms in fact do not contribute to final results due to being excluded from the sums in Eqs. (C16) and (C22). This exclusion of singular terms from the sums has been implemented by multiplying the perturbation coefficients with $(1-\delta_{n,l})$ and (or) $(1-\delta_{\alpha,\beta})$.

For the longitudinal part,

$$d_{nl;\alpha\beta}^{\chi_\parallel,y}(x) = -\frac{\alpha_\parallel\gamma_0}{2}\frac{k_BT}{k'vM_s}c_{Yn\alpha}c_{Yl\beta}I_{nl;\alpha\beta}^{\chi_\parallel}, \tag{C56}$$

where

$$I_{nl;\alpha\beta}^{\chi_\parallel} = \int_0^1 dy y^2\left[3\left(y^2-y_e^2\right)+2y^2\right]y^2\mathcal{Y}_{-n-1}(u_{-n-1,\alpha}y)\mathcal{Y}_{-l-1}(u_{-l-1,\beta}y), \tag{C57}$$

$$\simeq \frac{(-1)^{-(n+l)}}{u_{-n-1,\alpha}u_{-l-1,\beta}}\int_0^1 dy y^2\left[3\left(y^2-y_e^2\right)+2y^2\right]\cos\left(u_{-n-1,\alpha}y-(n+1)\frac{\pi}{2}\right)\cos(u_{-l-1,\beta}y-(l+1)\frac{\pi}{2}), \tag{C58}$$

which gives

$$
\begin{aligned}
I^{\chi_\parallel}_{nl;\alpha\beta} = {} & \frac{(-1)^{-(n+l)}}{u_{-n-1,\alpha}u_{-l-1,\beta}}\left(\frac{1}{2\pi^5}\right)\left(\frac{80(-1)^{\alpha+\beta}\pi(-24+4\alpha^2\pi^2+4\beta^2\pi^2+l^2\pi^2+4\beta(l-n)\pi^2)}{(2\alpha-2\beta-l+n)^4}\right)\\
& + \frac{(-1)^{-(n+l)}}{u_{-n-1,\alpha}u_{-l-1,\beta}}\left(-\frac{1}{2\pi^5}\right)\left(-\frac{80(-1)^{\alpha+\beta}\pi(-4\alpha(2\beta+l-n)\pi^2-2ln\pi^2+n^2\pi^2)}{(2\alpha-2\beta-l+n)^4}\right)\\
& + \frac{(-1)^{-(n+l)}}{u_{-n-1,\alpha}u_{-l-1,\beta}}\left(-\frac{1}{2\pi^5}\right)\left(\frac{80(-1)^{\alpha+\beta}\pi(-24+(4+2\alpha+2\beta+l+n)^2\pi^2)}{(4+2\alpha+2\beta+l+n)^4}\right)\\
& + \frac{(-1)^{-(n+l)}}{u_{-n-1,\alpha}u_{-l-1,\beta}}\left(-\frac{1}{2\pi^5}\right)\left(\frac{96(-1)^{\alpha+\beta}(2+2\beta+l)(2+2\alpha+n)\pi^3y_e^2}{(2\alpha-2\beta-l+n)^2(4+2\alpha+2\beta+l+n)^2}\right)\\
& + \frac{(-1)^{-(n+l)}}{u_{-n-1,\alpha}u_{-l-1,\beta}}\left(-\frac{1}{2\pi^5}\right)\left(\frac{3840\sin[(l-n)\frac{\pi}{2}]}{(2\alpha-2\beta-l+n)^5}+\frac{3840\sin[(l+n)\frac{\pi}{2}]}{(4+2\alpha+2\beta+l+n)^5}\right)\\
& + \frac{(-1)^{-(n+l)}}{u_{-n-1,\alpha}u_{-l-1,\beta}}\left(-\frac{1}{2\pi^5}\right)\times(-3\pi^2y_e^2)\left(-\frac{16\sin[(l-n)\frac{\pi}{2}]}{(2\alpha-2\beta-l+n)^3}-\frac{16\sin[(l+n)\frac{\pi}{2}]}{(4+2\alpha+2\beta+l+n)^3}\right).
\end{aligned}
\tag{C59}
$$

The last d coefficient comes from the response to magnetic fields, which for the static field is given by

$$
d^{H_0,y}_{nl;\alpha\beta}(x) = 2\alpha_\parallel\gamma_0 x\frac{k_BT}{k'vM_s}\int_0^1 dyy^2yu^y_{n\alpha}(y)u^y_{l\beta}(y) = 2\alpha_\parallel\gamma_0 x\frac{k_BT}{k'vM_s}I^{H_0}_{nl;\alpha\beta}c_{Yn\alpha}c_{Yl\beta},
\tag{C60}
$$

where

$$
\begin{aligned}
I^{H_0}_{nl;\alpha\beta} &= \int_0^1 dyy^3\mathcal{Y}_{-n-1}(u_{-n-1,\alpha}y)\mathcal{Y}_{-l-1}(u_{-l-1,\beta}y)\\
&\simeq \frac{(-1)^{-(n+l)}}{u_{-n-1,\alpha}u_{-l-1,\beta}}\int_0^1 dyy\cos\left(u_{-n-1,\alpha}y-(n+1)\frac{\pi}{2}\right)\cos\left(u_{-l-1,\beta}y-(l+1)\frac{\pi}{2}\right)\\
&= \frac{(-1)^{-(n+l)}}{u_{-n-1,\alpha}u_{-l-1,\beta}}\frac{2}{\pi^2}\left(\frac{(-1)^{\alpha+\beta}-\cos\left[(l-n)\frac{\pi}{2}\right]}{(2\alpha-2\beta-l+n)^2}\right)+\frac{(-1)^{-(n+l)}}{u_{-n-1,\alpha}u_{-l-1,\beta}}\frac{2}{\pi^2}\left(-\frac{(-1)^{\alpha+\beta}-\cos\left[(l+n)\frac{\pi}{2}\right]}{(4+2\alpha+2\beta+l+n)^2}\right),
\end{aligned}
\tag{C61}
$$

while for the ac field, the d coefficient is given by

$$
\begin{aligned}
d^{H_{\rm ac},y}_{nl;\alpha\beta}(x,t) &= 2\alpha_\parallel\gamma_0 x\frac{k_BT}{k'vM_s}\cos\omega t\int_0^1 dyy^2yu^y_{n\alpha}(y)u^y_{l\beta}(y) = +2\alpha_\parallel\gamma_0 x\frac{k_BT}{k'vM_s}I^{H_{\rm ac}}_{nl;\alpha\beta}c_{Yn\alpha}c_{Yl\beta}\cos\omega t,\\
I^{H_{\rm ac}}_{nl;\alpha\beta} &= \int_0^1 dyy^3\mathcal{Y}_{-n-1}(u_{-n-1,\alpha}y)\mathcal{Y}_{-l-1}(u_{-l-1,\beta}y)\\
&\simeq \frac{(-1)^{-(n+l)}}{u_{-n-1,\alpha}u_{-l-1,\beta}}\int_0^1 dyy\cos\left(u_{-n-1,\alpha}y-(n+1)\frac{\pi}{2}\right)\cos\left(u_{-l-1,\beta}y-(l+1)\frac{\pi}{2}\right),\\
&= \frac{(-1)^{-(n+l)}}{u_{-n-1,\alpha}u_{-l-1,\beta}}\frac{2}{\pi^2}\left(\frac{(-1)^{\alpha+\beta}-\cos[(l-n)\frac{\pi}{2}]}{(2\alpha-2\beta-l+n)^2}\right)+\frac{(-1)^{-(n+l)}}{u_{-n-1,\alpha}u_{-l-1,\beta}}\frac{2}{\pi^2}\left(-\frac{(-1)^{\alpha+\beta}-\cos[(l+n)\frac{\pi}{2}]}{(4+2\alpha+2\beta+l+n)^2}\right).
\end{aligned}
\tag{C62}
$$

We have verified numerically that the error from the discrepancy between the exact value of the integral from Eq. (C56) and its approximation from using Eq. (B23) is very small, less than 1%. This is because the largest deviation of the asymptotic function Eq. (B23) from the exact expression for the Bessel J function occurs at small $y \ll 1$. But this small y has reduced the contribution to the integral I_{nl} due to the y^3 term in I_{nl} in Eq. (C56).

On the other hand, using Eqs. (C8), (C9), and (C20), one obtains the following expression:

$$
e^{\alpha,x}_{nl}(y) = c_{Pl}\sum_{j=1,j\neq n}^{\infty}\frac{d^{\alpha,x}_{nj}(y)}{-n(n+1)+j(j+1)}c_{Pj}f^{\alpha}_{lj}(y),
\tag{C63}
$$

where $\alpha = H_0, \chi_\perp, H_{\rm ac}$ with

$$
\begin{aligned}
f^{\alpha}_{lj}(y) = {} & \frac{\alpha_\perp\gamma_0}{k'}\int_{-1}^{1}dxP_lx\frac{j(1-x^2)}{x^2-1}(xP_j(x)-P_{j-1}(x))\\
& \times\left(\delta_{\alpha,H_0}H_0+\delta_{\alpha,H_{0\rm ac}}H_{0\rm ac}\cos\omega t+\delta_{\alpha,\chi_\perp}\frac{M_s}{\chi_\perp}xy\right)y
\end{aligned}
\tag{C64}
$$

where $\delta_{\alpha,(H_0,\chi_\perp,H_{0\rm ac})}$ is the Kronecker delta function; e.g., $\delta_{\alpha,H_0}=1$ if $\alpha=H_0$ and zero otherwise. In the last part of the expression for $f^{\alpha}_{lj}(y)$ above, we have used the following identity for the derivative of Legendre polynomial:

$$
\frac{dP_j(x)}{dx} = \frac{j}{x^2-1}(xP_j(x)-P_{j-1}(x)).
\tag{C65}
$$

Explicit evaluation of the integral gives

$$f_{lj}^{H_0}(y) = -\frac{j\gamma_0\alpha_\perp H_0}{k'}\left[\frac{(l+j+1)g_{l,j}}{(2l+1)(2j+1)} - \frac{2\delta_{l,j-1}}{2l+1}\right]y, \tag{C66}$$

$$f_{lj}^{H_{\rm ac}}(y,t) = -\frac{j\gamma_0\alpha_\perp H_{\rm ac}(t)}{k'}\left[\frac{(l+j+1)g_{l,j}}{(2l+1)(2j+1)} - \frac{2\delta_{l,j-1}}{2l+1}\right]y, \tag{C67}$$

where $g_{l,j} = (1-\delta_{lj})\delta_{l,j\pm1}$ and

$$\begin{aligned} f_{lj}^{\chi_\perp}(y) = &-\frac{j\gamma_0 M_s\alpha_\perp}{k'\chi_\perp}\frac{\left[\delta_{lj}\left(\frac{2(l+1)^2}{2l+3}+\frac{2l^2}{2l-1}\right)\right]}{(2l+1)(2j+1)}y^2 \\ &-\frac{j\gamma_0 M_s\alpha_\perp}{k'\chi_\perp}\frac{\left[\frac{2(l+1)(l+2)}{2l+3}\delta_{l,j-2}+\frac{2(l-1)l}{2l-1}\delta_{j,l-2}\right]}{(2l+1)(2j+1)}y^2 \\ &+\frac{j\gamma_0 M_s\alpha_\perp}{k'\chi_\perp}(1-\delta_{l,j-1})\delta_{l,j-1\pm1}\frac{l+j}{(2l+1)(2j-1)}y^2. \end{aligned} \tag{C68}$$

Substituting $d_{nj}^{\chi,x}(y)$ from Eqs. (C49)–(C51) and f_{lj}^{χ} from Eqs. (C66)–(C68) above into Eq. (C63) and evaluating the sum over j gives

$$\begin{aligned} e_{nl}^{H_0,x}(y) = &-\frac{\alpha_\perp^2\gamma_0^2 k_B T H_0 y^2}{k'^2 v M_s}\frac{(n+1)(n+2)\delta_{n,l-2}}{(2n+3)\sqrt{(2n+1)(2n+5)}} \\ &-\frac{\alpha_\perp^2\gamma_0^2 k_B T H_0 y^2}{k'^2 v M_s}\frac{n(n-1)\delta_{n,l+2}}{(2n-1)\sqrt{(2n-3)(2n+1)}} \\ &+2\frac{\alpha_\perp^2\gamma_0^2 k_B T H_0 y^2}{k'^2 v M_s}\frac{n^2+n-1}{(2n-1)(2n+3)}\delta_{nl}, \end{aligned} \tag{C69}$$

$$\begin{aligned} e_{nl}^{H_{\rm ac},x}(y,t) = &-\frac{\alpha_\perp^2\gamma_0^2 k_B T H_{0\rm ac}(\cos\omega t - \omega\tau\sin\omega t)y^2}{k'^2 v M_s}\left[-2\frac{n^2+n-1}{(2n-1)(2n+3)}\delta_{nl}\right] \\ &-\frac{\alpha_\perp^2\gamma_0^2 k_B T H_{0\rm ac}(\cos\omega t - \omega\tau\sin\omega t)y^2}{k'^2 v M_s}\frac{1}{\sqrt{(2n+1)}}\left[\frac{(n+1)(n+2)\delta_{n,l-2}}{(2n+3)\sqrt{(2n+5)}}+\frac{n(n-1)\delta_{n,l+2}}{(2n-1)\sqrt{(2n-3)}}\right] \end{aligned} \tag{C70}$$

$$\begin{aligned} e_{nl}^{\chi_\perp,x}(y) = &-\frac{3\alpha_\perp^2\gamma_0^2 k_B T y^4}{2k'^2 v\chi_\perp\sqrt{(2n+1)(2l+1)}}\frac{n(n-1)(n-2)}{(2n-1)^2(2n-5)}\left(\frac{n-1}{2n-1}\delta_{l,n-2}+(n-3)\delta_{l,n-4}\right) \\ &+\frac{3\alpha_\perp^2\gamma_0^2 k_B T y^4}{2k'^2 v\chi_\perp(2n+1)}\left[\frac{(n+1)^2(n+2)^2(n+3)}{(2n+3)^3(2n+5)}+\frac{(n-1)^2n^2(n-2)}{(2n-3)(2n-1)^3}\right]\delta_{nl} \\ &+\frac{3\alpha_\perp^2\gamma_0^2 k_B T y^4}{2k'^2 v\chi_\perp\sqrt{(2n+1)(2l+1)}}\frac{(n+1)(n+2)^2(n+3)}{(2n+3)^2}\left(\frac{1}{(2n+3)(2n+7)}\delta_{l,n+2}-\frac{(n+4)}{(2n+5)(2n+7)}\delta_{l,n+4}\right). \end{aligned} \tag{C71}$$

One thing to observe is that the e^α coefficients are proportional to $\epsilon^\alpha(k_BT)^2$ where $\alpha = H_0, H_{\rm ac}, \chi_\perp$.

For the y part, we obtain for the transverse relaxation

$$\begin{aligned} e_{nl;\alpha\beta}^{\chi_\perp,y}(x) = &\frac{1}{k'}\frac{\alpha_\parallel\gamma_0 M_s}{\chi_\perp}c_{Yl\beta}(1-2x^2) \\ &\times\sum_{\beta'=0,\beta'\neq\alpha}^{\infty}\frac{d_{nn;\alpha\beta'}^{\chi_\perp,y}(x)c_{Yn\beta'}}{-\frac{n(n+1)}{u_{-n-1,\alpha}^2}+\frac{n(n+1)}{u_{-n-1,\beta'}^2}}G_{ln;\beta\beta'}^{\chi_\perp} \\ = &\frac{3\alpha_\parallel^2\gamma_0^2}{k'^2\chi_\perp}\frac{k_BT}{v}(1-x^2)(1-2x^2)\frac{c_{Yn\alpha}c_{Yl\beta}}{n(n+1)} \\ &\times\sum_{\beta'=0,\beta'\neq\alpha}^{\infty}\frac{u_{-n-1,\beta'}^2u_{-n-1,\alpha}^2}{\left(u_{-n-1,\alpha}^2-u_{-n-1,\beta'}^2\right)} \\ &\times(c_{Yn\beta'})^2 I_{nn;\alpha\beta'}^{\chi_\perp}G_{ln;\beta\beta'}^{\chi_\perp}, \end{aligned} \tag{C72}$$

where $I_{nn;\alpha\beta'}^{\chi_\perp}$ can be deduced from Eq. (C54) while

$$G_{ln;\beta\beta'}^{\chi_\perp} = \int_0^1 dy y^2 y^3 \mathcal{Y}_{-l-1}(u_{-l-1,\beta}y)\frac{d}{dy}(\mathcal{Y}_{-n-1}(u_{-n-1,\beta'}y)), \tag{C73}$$

and we have used Eq. (C6) for the eigenvalues. Employing again the relation Eq. (B30) as well as the following identity for the derivative of the Bessel function:

$$\frac{dJ_\nu(z)}{dz} = \frac{1}{2}(J_{\nu-1}(z)-J_{\nu+1}(z)), \tag{C74}$$

where $\nu = n+1/2$, we obtain

$$\begin{aligned} &G_{ln;\beta\beta'}^{\chi_\perp} \\ &= \frac{(-1)^{-(n+l)}\pi}{2\sqrt{u_{-l-1,\beta}u_{-n-1,\beta'}}}\int_0^1 dy y^3 J_{l+\frac{1}{2}}(z_{l\beta}) \\ &\times\left[-\frac{1}{2}J_{n+\frac{1}{2}}(z_{n\beta'})+\frac{z_{n\beta'}}{2}\left(J_{n-\frac{1}{2}}(z_{n\beta'})-J_{n+\frac{3}{2}}(z_{n\beta'})\right)\right], \end{aligned} \tag{C75}$$

where

$$z_{n\beta'} = u_{-n-1,\beta'}y,\ z_{l\beta} = u_{-l-1,\beta}y. \tag{C76}$$

Substituting the asymptotic expression and asymptotic approximation Eq. (B23) for the J's, we obtain

$$\begin{aligned} G_{ln;\beta\beta'}^{\chi_\perp} \simeq &\frac{(-1)^{-(n+l)}}{2(u_{-l-1,\beta}u_{-n-1,\beta'})}\int_0^1 dy y^2\cos\left(\Phi_{l,\beta}-\frac{\pi}{2}\right) \\ &\times\left[-\cos\left(\Phi_{n,\beta'}-\frac{\pi}{2}\right)+2u_{-n-1,\beta'}y\cos(\Phi_{n,\beta'})\right], \end{aligned} \tag{C77}$$

where $\Phi_{l(n),\beta(\beta')} = u_{-l(n)-1,\beta(\beta')}y - \frac{l(n)\pi}{2}$. The final result for $e^{\chi_\perp,y}_{nl;\alpha\beta}(x)$ can be written as

$$e^{\chi_\perp,y}_{nl;\alpha\beta}(x) = \frac{3\alpha_\parallel^2\gamma_0^2}{k'^2\chi_\perp}\frac{k_BT}{v}(1-x^2)(1-2x^2)\frac{c_{Yn\alpha}c_{Yl\beta}}{n(n+1)}E^{\chi_\perp}_{nl;\alpha\beta}$$
$$= 3\frac{\alpha_\parallel^2}{\alpha_\perp^2}\epsilon_y^{\chi_\perp}(1-x^2)(1-2x^2)\frac{c_{Yn\alpha}c_{Yl\beta}}{n(n+1)}E^{\chi_\perp}_{nl;\alpha\beta}, \tag{C78}$$

where $E^{\chi_\perp}_{nl;\alpha\beta}(x)$ is an analytical function in closed form involving special functions obtained from evaluating the sum over β' in Eq. (C72) which does give explicit result but is too tedious to be written out explicitly here.

The corresponding result for the longitudinal relaxation part is

$$e^{\chi_\parallel,y}_{nl;\alpha\beta}(x) = \frac{\alpha_\parallel\gamma_0 M_s}{2\chi_\parallel k'}\sum_{\beta'=0,\beta'\neq\alpha}^{\infty}\frac{c_{Yl\beta}d^{\chi_\parallel,y}_{nn;\alpha\beta'}(x)c_{Yn\beta'}}{-\frac{n(n+1)}{u^2_{-n-1,\alpha}}+\frac{n(n+1)}{u^2_{-n-1,\beta'}}}G^{\chi_\parallel}_{ln;\beta\beta'}$$
$$= -\frac{1}{k'^2}\frac{\alpha_\parallel^2\gamma_0^2k_BT}{4\chi_\parallel v}\frac{c_{Yn\alpha}c_{Yl\beta}}{n(n+1)}\sum_{\beta'=0,\beta'\neq\alpha}^{\infty}\frac{u^2_{-n-1,\beta'}u^2_{-n-1,\alpha}}{(u^2_{-n-1,\alpha}-u^2_{-n-1,\beta'})}(c_{Yn\beta'})^2I^{\chi_\parallel}_{nn;\alpha\beta'}G^{\chi_\parallel}_{ln;\beta\beta'}$$
$$= -\frac{\alpha_\parallel^2}{4\alpha_\perp^2}\epsilon_y^{\chi_\parallel}\frac{c_{Yn\alpha}c_{Yl\beta}}{n(n+1)}\sum_{\beta'=0,\beta'\neq\alpha}^{\infty}\frac{u^2_{-n-1,\beta'}u^2_{-n-1,\alpha}}{(u^2_{-n-1,\alpha}-u^2_{-n-1,\beta'})}(c_{Yn\beta'})^2I^{\chi_\parallel}_{nn;\alpha\beta'}G^{\chi_\parallel}_{ln;\beta\beta'}, \tag{C79}$$

where $I^{\chi_\perp}_{nn;\alpha\beta'}$ can be deduced from Eq. (C59) while

$$G^{\chi_\parallel}_{ln;\beta\beta'} = \int_0^1 dyy^2y^3(y^2-y_e^2)\mathcal{Y}_{-l-1}(u_{-l-1,\beta}y)\frac{\partial}{\partial y}(\mathcal{Y}_{-n-1}(u_{-n-1,\beta'}y))$$
$$\simeq \frac{(-1)^{-(n+l)}}{2(u_{-l-1,\beta}u_{-n-1,\beta'})}\int_0^1 dyy^2(y^2-y_e^2)\cos\left(\Phi_{l,\beta}-\frac{\pi}{2}\right)\left[-\cos\left(\Phi_{n,\beta'}-\frac{\pi}{2}\right)+2u_{-n-1,\beta'}y\cos(\Phi_{n,\beta'})\right], \tag{C81}$$

where $\Phi_{l(n),\beta(\beta')} = u_{-l(n)-1,\beta(\beta')}y - \frac{l(n)\pi}{2}$, with the final result for which the analytical expression is too long to be written explicitly here.

For the e coefficient describing the response to the magnetic fields

$$e^{H_\alpha,y}_{nl;\alpha\beta}(x) = -\frac{\alpha_\parallel\gamma_0}{k'}H_\alpha xc_{Yl\beta}\sum_{\beta'=0,\beta'\neq\alpha}^{\infty}\frac{d^{H_\alpha,y}_{nn;\alpha\beta'}(x)c_{Yn\beta'}}{-\frac{n(n+1)}{u^2_{-n-1,\alpha}}+\frac{n(n+1)}{u^2_{-n-1,\beta'}}}G^{H_\alpha}_{ln;\beta\beta'}$$
$$= -2\frac{\alpha_\parallel^2\gamma_0^2k_BT}{k'^2vM_s}H_\alpha x^2\frac{c_{Yn\alpha}c_{Yl\beta}}{n(n+1)}\sum_{\beta'=0,\beta'\neq\alpha}^{\infty}\frac{u^2_{-n-1,\beta'}u^2_{-n-1,\alpha}}{(u^2_{-n-1,\alpha}-u^2_{-n-1,\beta'})}(c_{Yn\beta'})^2I^{H_\alpha}_{nn;\alpha\beta'}G^{H_\alpha}_{ln;\beta\beta'}$$
$$= -2\frac{\alpha_\parallel^2}{\alpha_\perp^2}\epsilon_y^{H_\alpha}x^2\frac{c_{Yn\alpha}c_{Yl\beta}}{n(n+1)}\sum_{\beta'=0,\beta'\neq\alpha}^{\infty}\frac{u^2_{-n-1,\beta'}u^2_{-n-1,\alpha}}{(u^2_{-n-1,\alpha}-u^2_{-n-1,\beta'})}(c_{Yn\beta'})^2I^{H_\alpha}_{nn;\alpha\beta'}G^{H_\alpha}_{ln;\beta\beta'}, \tag{C82}$$

where $H_\alpha = H_0, H_{\rm ac}$, and $I^H_{nn;\alpha\beta'}$ can be deduced from Eqs. (C61)–(C62) while

$$G^{H_\alpha}_{ln;\beta\beta'} = \int_0^1 dyy^4\mathcal{Y}_{-l-1}(u_{-l-1,\beta}y)\frac{\partial}{\partial y}(\mathcal{Y}_{-n-1}(u_{-n-1,\beta'}y))$$
$$\simeq \frac{(-1)^{-(n+l)}}{2(u_{-l-1,\beta}u_{-n-1,\beta'})}\int_0^1 dyy\cos\left(u_{-l-1,\beta}y-(l+1)\frac{\pi}{2}\right)\left[-\cos\left(u_{-n-1,\beta'}y-(n+1)\frac{\pi}{2}\right)\right]$$
$$+\frac{(-1)^{-(n+l)}}{2(u_{-l-1,\beta}u_{-n-1,\beta'})}\int_0^1 dyy\cos\left(u_{-l-1,\beta}y-(l+1)\frac{\pi}{2}\right)[u_{-n-1,\beta'}y(\cos(\Phi_{n,\beta'})-\cos(\Phi_{n,\beta'}-\pi))], \tag{C83}$$

where $\Phi_{n,\beta'} = u_{-n-1,\beta'}y - \frac{n\pi}{2}$.

The last coefficient $h_{nl;\alpha\beta}$ from Eq. (C27) is evaluated in similar manner, giving

$$h_{nl;\alpha\beta} = \int_0^1 dyy^2c_{Yn\alpha}\mathcal{Y}_{-n-1}(u_{-n-1,\alpha}y)c_{Yl\beta}\mathcal{Y}_{-l-1}(u_{-l-1,\beta}y) \simeq \frac{(-1)^{1-(n+l)}c_{Yn\alpha}c_{Yl\beta}}{\pi u_{-n-1,\alpha}u_{-l-1,\beta}}\left(\frac{\sin[(-\alpha+\beta)\pi]-\sin[(-l+n)\frac{\pi}{2}]}{(2\alpha-2\beta-l+n)}\right)$$
$$\simeq \frac{(-1)^{1-(n+l)}c_{Yn\alpha}c_{Yl\beta}}{\pi u_{-n-1,\alpha}u_{-l-1,\beta}}\left(\frac{\sin[(2+\alpha+\beta)\pi]+\sin[(l+n)\frac{\pi}{2}]}{(4+2\alpha+2\beta+l+n)}\right), \tag{C84}$$

where the zeros $u_{-n-1,\alpha}, u_{-l-1,\beta}$ can be deduced from Eq. (C55).

It is to be noted that all the coefficients $e^{\xi;y}_{nl}(x)$ are of first order in ϵ^{ξ}_{y}, where $\xi = \chi_{\perp}, \chi_{\parallel}, H_0, H_{\rm ac}$. Substituting the above results for $d^{\xi,y}_{nl}(x)$ and $e^{\xi,y}_{nl}(x)$, we obtain the first lowest order correction to the eigenvalue for the y part, which directly gives the decay rate due to thermal diffusion

$$\begin{aligned}\overline{\lambda}^{y}_{n\alpha} &= \lambda^{y}_{n\alpha} + \epsilon^{\xi}_{y}\mu^{\xi;y}_{n\alpha}(x) + O(\epsilon^2)\\ &= \lambda^{y}_{n\alpha} + \epsilon^{\xi}_{\xi;y}\mu^{\xi;y}_{n\alpha}(x) + O(\epsilon^2)\\ &= \lambda^{y}_{n\alpha} + \epsilon^{\xi}_{y}(d^{\xi;y}_{nn;\alpha\alpha}(x) - e^{\xi;y}_{nn;\alpha\alpha}(x)) + O(\epsilon^2)\\ &\simeq \lambda^{y}_{n\alpha} + \epsilon^{\xi}_{y}d^{\xi;y}_{nn;\alpha\alpha}(x) + \tilde{O}(\epsilon^2) \qquad \text{(C85)}\end{aligned}$$

and with Eq. (C6),

$$-\frac{n(n+1)}{\overline{u}^2_{-n-1,\alpha}} \simeq -\frac{n(n+1)}{u^2_{-n-1,\alpha}} + \epsilon^{\xi}_{y}d^{\xi;y}_{nn;\alpha\alpha}(x) + \tilde{O}(\epsilon^2), \qquad \text{(C86)}$$

where summation over ξ is implied. Solving for $\overline{u}^2_{-n-1,\alpha}$ and noting that $p_{n\alpha} = u^2_{-n-1,\alpha}k'$, we obtain

$$\begin{aligned}\overline{p}_{n\alpha}(x) &= p_{n\alpha}\left(1 + \frac{u^2_{-n-1,\alpha}}{n(n+1)}\epsilon^{\xi}_{y}d^{\xi;y}_{nn;\alpha\alpha}(x)\right)\\ &= p_{n\alpha}\left(1 - \frac{u^2_{-n-1,\alpha}}{n(n+1)}\epsilon^{\xi}_{y}|d^{\xi;y}_{nn;\alpha\alpha}(x)|\right), \qquad \text{(C87)}\end{aligned}$$

provided $d^{y}_{nn;\alpha\alpha}(x) < 0$.

[1] L. Landau and E. Lifshitz, Phys. Z. Sowjetunion **8**, 153 (1935).
[2] T. L. Gilbert, IEEE Trans. Magn. **40**, 3443 (2004).
[3] D. A. Garanin, Phys. Rev. B **55**, 3050 (1997).
[4] A. Kirilyuk, A. V. Kimel, and Th. Rasing, Rev. Mod. Phys. **82**, 2731 (2010).
[5] U. Atxitia, D. Hinzke, and U. Nowak, J. Phys. D: Appl. Phys. **50**, 033003 (2017).
[6] H. Kachkachi and D. A. Garanin, Physica A **291**, 485 (2001).
[7] D. A. Garanin and O. Chubykalo-Fesenko, Phys. Rev. B **70**, 212409 (2004).
[8] I. Makhfudz, Phys. Rev. B **89**, 024401 (2014).
[9] M.-C. Ciornei, J. M. Rubí, and J.-E. Wegrowe, Phys. Rev. B **83**, 020410(R) (2011).
[10] R. Mondal, M. Berritta, A. K. Nandy, and P. M. Oppeneer, Phys. Rev. B **96**, 024425 (2017).
[11] K. Neeraj, N. Awari, S. Kovalev, D. Polley, N. Zhou Hagström, S. S. P. K. Arekapudi, A. Semisalova, K. Lenz, B. Green, J.-C. Deinert, I. Ilyakov, M. Chen, M. Bawatna, V. Scalera, M. d'Aquino, C. Serpico, O. Hellwig, J.-E. Wegrowe, M. Gensch, and S. Bonetti, Nat. Phys. **17**, 245 (2021).
[12] E. Olive, Y. Lansac, and J.-E. Wegrowe, Appl. Phys. Lett. **100**, 192407 (2012).
[13] E. Olive, Y. Lansac, M. Meyer, M. Hayoun, and J.-E. Wegrowe, J. Appl. Phys. **117**, 213904 (2015).
[14] I. Makhfudz, E. Olive, and S. Nicolis, Appl. Phys. Lett. **117**, 132403 (2020).
[15] A. M. Lomonosov, V. V. Temnov, and J.-E. Wegrowe, Phys. Rev. B **104**, 054425 (2021).
[16] S. V. Titov, W. T. Coffey, Yu. P. Kalmykov, M. Zarifakis, and A. S. Titov, Phys. Rev. B **103**, 144433 (2021).
[17] K. Neeraj, M. Pancaldi, V. Scalera, S. Perna, M. d'Aquino, C. Serpico, and S. Bonetti, Phys. Rev. B **105**, 054415 (2022).
[18] R. F. L. Evans, D. Hinzke, U. Atxitia, U. Nowak, R. W. Chantrell, and O. Chubykalo-Fesenko, Phys. Rev. B **85**, 014433 (2012).
[19] U. Atxitia, O. Chubykalo-Fesenko, R. W. Chantrell, U. Nowak, and A. Rebei, Phys. Rev. Lett. **102**, 057203 (2009).
[20] E. Beaurepaire, J.-C. Merle, A. Daunois, and J.-Y. Bigot, Phys. Rev. Lett. **76**, 4250 (1996).
[21] J. Hohlfeld, E. Matthias, R. Knorren, and K. H. Bennemann, Phys. Rev. Lett. **78**, 4861 (1997).
[22] B. Koopmans, M. van Kampen, J. T. Kohlhepp, and W. J. M. de Jonge, Phys. Rev. Lett. **85**, 844 (2000).
[23] J. Hohlfeld, Th. Gerrits, M. Bilderbeek, Th. Rasing, H. Awano, and N. Ohta, Phys. Rev. B **65**, 012413 (2001).
[24] H.-S. Rhie, H. A. Durr, and W. Eberhardt, Phys. Rev. Lett. **90**, 247201 (2003).
[25] A. V. Kimel, A. Kirilyuk, P. A. Usachev, R. V. Pisarev, A. M. Balbashov, and Th. Rasing, Nature **435**, 655 (2005).
[26] F. Hansteen, A. Kimel, A. Kirilyuk, and Th. Rasing, Phys. Rev. Lett. **95**, 047402 (2005).
[27] M. Cinchetti, M. Sánchez Albaneda, D. Hoffmann, T. Roth, J.-P. Wustenberg, M. Krauß, O. Andreyev, H. C. Schneider, M. Bauer, and M. Aeschlimann, Phys. Rev. Lett. **97**, 177201 (2006).
[28] C. D. Stanciu, F. Hansteen, A. V. Kimel, A. Kirilyuk, A. Tsukamoto, A. Itoh, and Th. Rasing, Phys. Rev. Lett. **99**, 047601 (2007).
[29] J. Hohlfeld, C. D. Stanciu, and A. Rebei, Appl. Phys. Lett. **94**, 152504 (2009).
[30] K. Vahaplar, A. M. Kalashnikova, A. V. Kimel, D. Hinzke, U. Nowak, R. Chantrell, A. Tsukamoto, A. Itoh, A. Kirilyuk, and Th. Rasing, Phys. Rev. Lett. **103**, 117201 (2009).
[31] I. Radu, K. Vahaplar, C. Stamm, T. Kachel, N. Pontius, H. A. Durr, T. A. Ostler, J. Barker, R. F. L. Evans, R. W. Chantrell, A. Tsukamoto, A. Itoh, A. Kirilyuk, Th. Rasing, and A. V. Kimel, Nature **472**, 205 (2011).
[32] M. Wietstruk, A. Melnikov, C. Stamm, T. Kachel, N. Pontius, M. Sultan, C. Gahl, M. Weinelt, H. A. Durr, and U. Bovensiepen, Phys. Rev. Lett. **106**, 127401 (2011).
[33] J. H. Mentink, J. Hellsvik, D. V. Afanasiev, B. A. Ivanov, A. Kirilyuk, A. V. Kimel, O. Eriksson, M. I. Katsnelson, and Th. Rasing, Phys. Rev. Lett. **108**, 057202 (2012).
[34] C.-H. Lambert, S. Mangin, B. S. D. Ch. S. Varaprasad, Y. K. Takahashi, M. Hehn, M. Cinchetti, G. Malinowski, K. Hono, Y. Fainman, M. Aeschlimann, and E. E. Fullerton, Science **345**, 1337 (2014).
[35] O. Chubykalo-Fesenko, U. Nowak, R. W. Chantrell, and D. Garanin, Phys. Rev. B **74**, 094436 (2006).
[36] W. F. Brown, Jr., Phys. Rev. **130**, 1677 (1963).
[37] D. A. Garanin, V. V. Ishchenko, and L. V. Panina, Teor. Mat. Fiz. **82**, 169, (1990); Theor. Math. Phys. USSR **82**, 169 (1990).
[38] N. Kazantseva, D. Hinzke, R. W. Chantrell, and U. Nowak, Europhys. Lett. **86**, 27006 (2009).

[39] R. Courant and D. Hilbert, *Methods of Mathematical Physics* (Interscience Publishers, Inc., New York, 1953), Vol. 1.
[40] M. J. Alizadeh, H. Kariminezhad, A. S. Monfared, A. Mostafazadeh, H. Amani, F. Niksirat, and R. Pourbagher, Mater. Res. Express **6**, 065025 (2019).
[41] V. Singh, M. S. Seehra, and J. Bonevich, J. Appl. Phys. **105**, 07B518 (2009).
[42] F. Bødker, S. Mørup, M. S. Pedersen, P. Svedlindh, G. T. Jonsson, J. L. Garcia-Palacios, and F. J. Lazaro, J. Magn. Magn. Mater. **177-181**, 925 (1998).
[43] W. Wernsdorfer, E. B. Orozco, K. Hasselbach, A. Benoit, B. Barbara, N. Demoncy, A. Loiseau, H. Pascard, and D. Mailly, Phys. Rev. Lett. **78**, 1791 (1997).
[44] W. D. Corner, W. C. Roe, and K. N. R. Taylor, Proc. Phys. Soc. **80**, 927 (1962).
[45] U. Köbler, J. Englich, O. Hupe, and J. Hesse, Phys. B: Conden. Matter **339**, 156 (2003).
[46] M. S. S. Brooks and D. A. Goodings, J. Phys. C: Solid State Phys. **1**, 1279 (1968).
[47] C. D. Graham, Jr., Phys. Rev. **112**, 1117 (1958).
[48] N. L. Brukhatov and L. V. Kirenksy, Physikalische Zeitschrift der Sowjetunion. Band 12, Heft 5 (1937).
[49] D. M. Paige, B. Szpunar, and B. K. Tanner, J. Magn. Magn. Mater. **44**, 239 (1984).
[50] W. Sucksmith and J. E. Thompson, Proc. R. Soc. London A **225**, 362 (1954).
[51] J. F. Elliott, S. Legvold, and F. H. Spedding, Phys. Rev. **91**, 28 (1953).
[52] J. Crangle and G. M. Goodman, Proc. R. Soc. London A **321**, 477 (1971).
[53] V. A. Bautin, A. G. Seferyan, M. S. Nesmeyanov, and N. A. Usov, AIP Adv. **7**, 045103 (2017).
[54] For examples, see Wiki pages on Legendre polynomials and Bessel functions, especially spherical Bessel functions.